CHALMERS

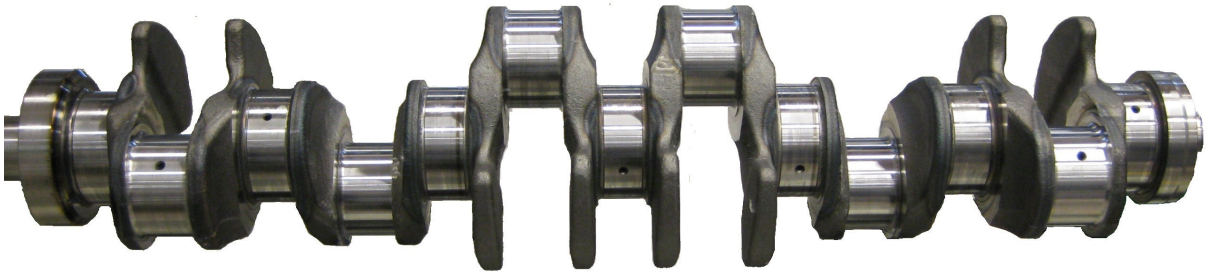

Correlation between material properties, grinding effects and Barkhausen noise measurements for two crankshaft steels

Master's Thesis in Applied Physics

MARIE DOVERBO

Department of Materials and Manufacturing Technology
Division of Surface and Microstructure Engineering
CHALMERS UNIVERSITY OF TECHNOLOGY
Göteborg, Sweden 2012
Master's Thesis

MASTER'S THESIS

Correlation between material properties, grinding effects and Barkhausen noise measurements for two crankshaft steels

Master's Thesis in Applied Physics

MARIE DOVERBO

Department of Materials and Manufacturing Technology
Division of Surface and Microstructure Engineering
CHALMERS UNIVERSITY OF TECHNOLOGY

Göteborg, Sweden 2012

Correlation between material properties, grinding effects and Barkhausen noise measurements for two crankshaft steels
MARIE DOVERBO

Master's Thesis
Department of Materials and Manufacturing Technology
Division of Surface and Microstructure Engineering
Chalmers University of Technology
SE-412 96 Göteborg
Sweden
Telephone: + 46 (0)31-772 1000

Cover:
One of the crankshafts examined in this thesis.

Chalmers Reproservice
Göteborg, Sweden 2012

Correlation between material properties, grinding effects and Barkhausen noise measurements for two crankshaft steels
Master's Thesis in Applied Physics
MARIE DOVERBO
Department of Materials and Manufacturing Technology
Division of Surface and Microstructure Engineering
Chalmers University of Technology

Abstract

The crankshaft steel of two suppliers has been shown to yield differing Barkhausen measurements despite corresponding material specifications and identical manufacturing. In this thesis the reason for this discrepancy is investigated and an hypothesis regarding its cause is formulated. The conclusions are reached through experimental work, wherein the material properties of the two steels are compared. The found difference in ductility is related to the difference in Barkhausen Noise Amplitude (BNA) through the grinding process such that the increased ductility is believed to increase the chip build up in the grinding wheel, thus resulting in higher grinding temperature. This would increase the risk for grinding burns and moves the residual stresses towards tensile, which changes the BNA. Suggestions for future work all concern the verification of this hypothesis.

Keywords

Barkhausen effect, Barkhausen noise, grinding, crankshafts, ductility, low carbon steel

Contents

Acknowledgements

I would like to thank the Basic Engine group at Scania Materials Technology for their generous help and for answering all of my thousands of questions. Special thanks to my advisor Lars Hammerström for all of his support and valuable feedback during this thesis work. I also want to thank Stig Ragnarsson of SlipNaxos and Roope Roininen at Scania crankshaft production for teaching me everything I know about grinding, and Per Lundin of Stresstech and Ronnie Kvist for being the Barkhausen gurus. Finally I would like to thank Peter Krajnik of KTH for letting me use his results for some of my conclusions in this thesis, and Lars Nyborg for being my supervisor.

Göteborg June 2012
Marie Doverbo

Abbreviations

Some abbreviations will be used throughout the text to shorten it and make it more readable. These will be explained below.

BN - Barkhausen Noise (especially referring to the measurement method)
BNA - Barkhausen Noise Amplitude
S1 - Supplier 1
S2 - Supplier 2

Specimen naming

During this project several specimens were manufactured for several test methods. The specimens were all named after the location they were taken from to simplify both comparison amongst each other and with the Barkhausen reference curves. The naming system is explained below.

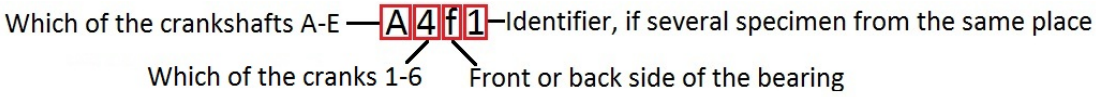

1 Introduction

To grind a crankshaft is not as easy as one might think.

This introduction will describe the problem setting for this thesis project, as well as provide a short description of the methodology used and the structure of the thesis.

1.1 Background

Scania CV AB is one of the leading manufacturers of heavy trucks, buses, and engines for industrial and marine applications. In 2011 a little over 70 000 units were sold, each containing one crankshaft.[1] The crankshafts are bought from two suppliers in forged condition, while the hardening and machining is performed by Scania.

The crankshaft is subjected to large stresses and its structural strength is therefore of great importance. The most important feature is the hardness of the bearings' surfaces as they have to resist the forces and wear from the connecting rods. At the same time they must be grinded to a certain geometry in the shortest possible amount of time, risking grinding burns that destroy the surface properties. Thus the crankshafts are checked for grinding burns and other defects when they are finished. One method that has proven to be both effective and non-destructive is Barkhausen Noise Measurement.[2;3]

In short the Barkhausen method returns a dimensionless number based on a magnetization sequence, and generally a lower number is better. The goal is to measure this number around the bearing and if it exceeds a certain threshold value at any point on the surface then we know that the shaft has a grinding burn at that location. When trying to determine this threshold value it was discovered that among two suppliers, crankshafts from one had significantly lower average Barkhausen Noise measurements than crankshafts from the other. How is that? Do the materials react differently to the grinding so that one material is actually more likely to burn? Or do the Barkhausen method, which is very sensitive to variations in certain material parameters, simply pick up on a difference in one material parameter that has no effect on the grinding performance?

1.2 Purpose, scope and limitations

The purpose of this thesis is to find the reason for the difference in the results from the Barkhausen measurements of the crankshafts from two of Scania's suppliers. The crankshafts are compared with regard to material properties and grinding performance and the differences found are related to theory explaining the behavior of the Barkhausen effect. Most attention is given to the crankshafts' washers since this is where grinding burns occur, if any.

Only crankshafts from the two suppliers named S1 and S2 are examined. Also the purpose was only to identify differences in the material and their qualitative effect on the Barkhausen measurement method; no direct evaluation or optimization of the grinding process would be done. Because of the broadness of scope, this thesis is more of a pre-study and there have been no time for any full scale test series. The purpose is only that this thesis study will serve as an orientation in the preparation of future work on the subject.

1.3 Method

Both a literature study and experimental work were performed during this master thesis project. The literature study initially covered the Barkhausen effect with adherent measurement methods and the effect various material parameters have on the measurements, as well as the very basics of grinding technology. Further information retrieval was carried out as the need for it arose and the sources were partly by personal communication.

Which experimental methods that should be used was to a large extent not possible to define beforehand. The purpose of the experimental studies was therefore to identify the possible causes for differences in Barkhausen Noise measurements for the materials. Thus, the starting point would have to be a handful of standard tests, and every following experiment was chosen based on the results from the previous ones. This meant that the experimental work was divided into phases between which information retrieval took place. The information retrieval concerned the implications of the results and which experiments to go forward with.

1.4 Thesis outline

In chapter 2 Theory some basic theory needed to follow the topic of this thesis is presented. This covers magnetism and the Barkhausen effect, grinding, and finally how various material parameters are correlated and how these could connect to the grinding performance and the Barkhausen measurements.

Following this the studied components, i.e. the crankshafts, are presented in chapter 3 Crankshafts.

Then follows a chapter covering all the experiments and results of this thesis project. Because of the methodology of the project, the experiments and results are divided into three parts, each followed by a discussion. Chapter 4 (part 1) covers the Barkhausen measurements as well as the measurement of each crankshaft's hysteresis curve, both used as reference throughout the project. Chapter 5 (part 2) presents a first set of experiments that were decided on already in the planning stage as they are broad and easy standard tests. These are measurements of hardness, residual stresses and chemical composition, and a microstructure analysis. Chapter 6 (part 3) finally contains a follow up set of experiments providing a closer examination of possible differences found in part 2. This set comprises torsion testing, Charpy impact testing and tensile testing of materials in hardened condition.

Finally all conclusions and suggestions for further studies are presented in chapter 7 Conclusion.

2 Theory

In this section some basic theory useful for the understanding of this thesis study is presented. The topics will concern various relevant material parameters and their interactions, the basics of grinding as well as the history, application and theoretical descriptions of the Barkhausen noise measurement method. Finally, a summary of previous and parallel related studies at Scania will be included.

2.1 Some mechanical properties of metals

The interactions of various mechanical and microstructural properties of metals are complex but a summary will be given below. The text will define and explain the concepts of elasticity, plasticity, ductility, hardness and residual stresses. The mechanical properties arise from the material microstructure, which also affect the magnetic properties discussed in section 2.3. The source for this section is the book "Mechanical Behavior of Materials" by M. Meyers and K. Chawla.[4]

2.1.1 Elastic versus plastic

The definition of an elastic material is that it can return to its original shape after it has been deformed. A plastic material does not return but maintains its deformed shape. Most metals exhibit some mix of both elasticity and plasticity, being elastic for small deformations but deforming permanently for larger strains. In the elastic regime the amount of strain σ in a metal is proportional to the applied stress ϵ according to Hooke's Law $\sigma = E\epsilon$, where E is the proportionality constant Young's modulus. E can be measured with a tensile test.

The result from a tensile test usually looks like figure 2.1. The elastic part is the straight portion in the beginning and Young's modulus is the slope. The point where the curve deviates from the linear is called the *yield point*, and this marks the onset of plasticity. The maximum point on the curve is called the *ultimate tensile strength* and after this point a neck is formed on the test bar. The neck gets narrower until the test bar finally breaks, lowering the force needed to continue straining although the true stress increases. The area under the curve correlates to the metal's *toughness*, which represents the total amount of energy the test bar can absorb before it breaks. The *area reduction*, that is the relative difference in area of the test bar before and after the test, and the *elongation to fracture* are measurements of the ductility of the metal. Unloading the test bar during the tensile test leads to that the bar recovers elastically (linearly, sloping as Young's modulus) to zero stress but at a residual strain larger than zero. Continuing the tensile test again results in an elastic strain up until the stress where the test was paused and subsequent plastic deformation.

2.1.2 Ductility

This is the metal's ability to deform under tensile stress. The ability to deform under compressive stress is called malleability and will not be discussed. The ductility is mostly related to the metal's ability to shear, and ductile materials that fracture do so because they fail in shear. Deforming or shearing a metal means that the atoms must slide past one another, thereby destroying the ordered lattice. The sliding is accommodated by *dislocations*, certain crystal defects. Figure 2.2 depicts the two basic kinds of dislocations: edge

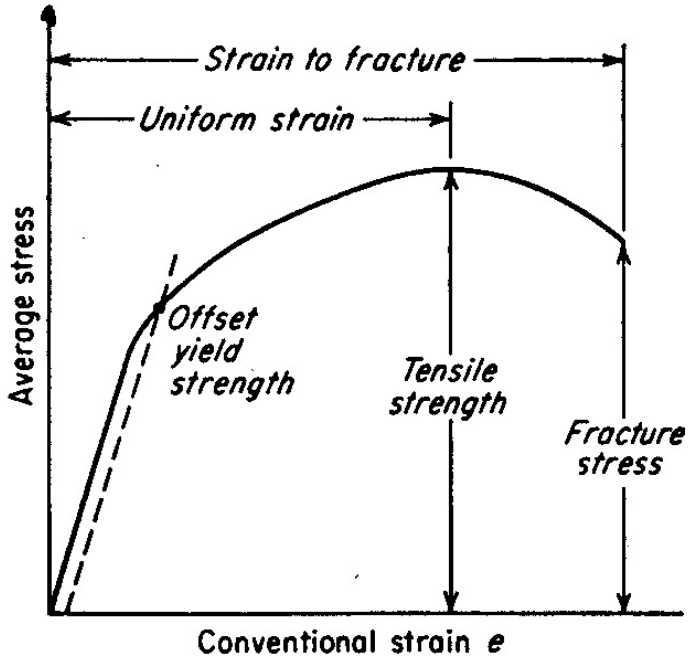

Figure 2.1: A typical stress-strain curve from a tensile stress. The relationship is linear until the onset of plasticity at the yield point. Necking begins after the curve's maximum point. *Picture: www.keytometals.com/Article107.htm*

and screw dislocations. These defects allow parts of atomic planes to slide without having to move the entire plane. In effect dislocations can be viewed as carriers of deformation.

As long as the dislocations are free to move the metal can deform plastically. Dislocations are created and sometimes annihilated in e.g. grain boundaries or around inclusions, and the more deformed the piece of metal becomes the more dislocations it contains. After enough deformation the dislocation density is so high that the dislocations begin to entangle and are unable to move. They can also pile up against inclusions, grain boundaries and other defects which also stops their motion. When the dislocations cannot move the metal cannot deform but stiffens, and ultimately it fractures.

The ductility of a metal depends on the temperature and strain rate. When the temperature is too low or the strain rate too high then the dislocations cannot move fast enough to enable plastic deformation. Instead of a viscous ductile fracture the metal cracks in brittle fracture. The temperature where 50% of the fracture is ductile and 50% brittle is called the *Ductile Brittle Transition Temperature*, and the DBTT is different for each material. Materials like steel, having body-centered cubic crystal structure, show characteristic DBTT. The percentage ductile fracture is easily determined by visual inspection of the fracture surfaces, where the brittle fracture occurs along the edges of a broken test piece.

2.1.3 Residual stresses

Often metals contain inner stresses although the piece of material is not loaded by any external loads. These stresses are either tensile or compressive, and the sign convention is

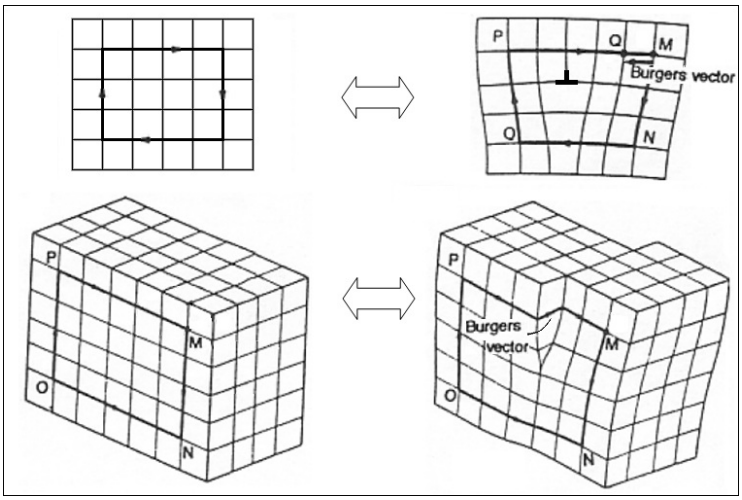

Figure 2.2: Top: edge dislocation. Bottom: screw dislocation. The Burger's vector is a mathematical description of the particular dislocation. *Picture: Javier Vílchez through Wikimedia Commons.*

that tensile stresses are counted as positive stresses and compressive as negative. These stresses vary throughout the metal but the sum of all residual stresses is always zero, or else the piece would be accelerating. The stress state can be altered in two main ways; mechanical action and heat treatment.

The most important loading case for crankshafts is bending. Bending a bar of metal produces compressive stresses on the inner side and tensile stresses on the outer side. These are not true residual stresses as they do not exist without the load, but the stress is identical. If the bar is bent until it plasticizes the stress state is altered permanently, and this is a case where the stress state is due to mechanical action.

Heating the metal slightly releases residual stresses as the increased temperature allows the atoms to relax into more "comfortable" positions. Surface hardening - heating the surface above its austenitization temperature and then quenching - produces compressive stresses in the martensitic surface layer and tensile stresses below. This is because the volume expansion accompanying the martensitic transformation is restricted by the untransformed material beneath. The compressive stresses in the surface make the metal hard and prevents crack initiation and growth. Here a desired residual stress state is created with heat treatment.

2.1.4 Hardness

Hardness is a measure of a material's resistance to plastic deformation when exposed to a force. It is not a fundamental property of a solid but is a function of the metal's elastic stiffness and yield strength, plasticity, strain, strength, toughness, and viscoelasticity. The hardness of a metal is often tested through indentation testing, where a hard tip is pressed with a constant force against a flat surface.

A number of techniques to make a metal's hardness increase exists. All of them revolves around hindering the motion of dislocations. Decreasing the grain size increases the hardness as the boundaries promotes dislocation creation and stops their motion (down to a critical grain-size beyond which the hardness decreases again). Alloying that create interstitials, precipitates or inclusions also lead to locking of dislocations.

2.2 Outer diameter cylindrical grinding

Grinding is abrasive cutting, a machining process useful in making parts meet tight tolerances. The cutting itself is done by thousands of grains bonded together into a grinding wheel, the matrix consisting of rubber, ceramics, plastics or even metal depending on application. The matrix is adjusted so that it is strong enough to hold the grits but still porous enough to enable transport of cooling fluid to and chips away from the working area. In outer diameter cylindrical grinding the workpiece is mounted on two axial pins around which it is rotated by an engine. The grinding wheel is brought into contact with the workpiece while it is rotated at another speed.

Grinding is different from many other cutting techniques in a number of ways. Firstly, rather than one large sharp edge thousands of small irregular edges are used producing very small chips. Secondly the edges have highly negative rake angles. Finally the cutting is performed at very high speeds (hundreds of km/h).

The action of the grinding wheel on the workpiece is shown in figure 2.3. When a piece of grit is brought into contact with the workpiece it starts by rubbing a short distance on the surface as the normal force F_n builds up. When the pressure is high enough the grit plows down into the material, pushing material in front of it. This pushing produces shear forces in the material. Finally a chip starts to form and the grit now cuts through the material. The negative rake angle gives a stronger edge to the grit, but builds up higher shear forces in the workpiece.

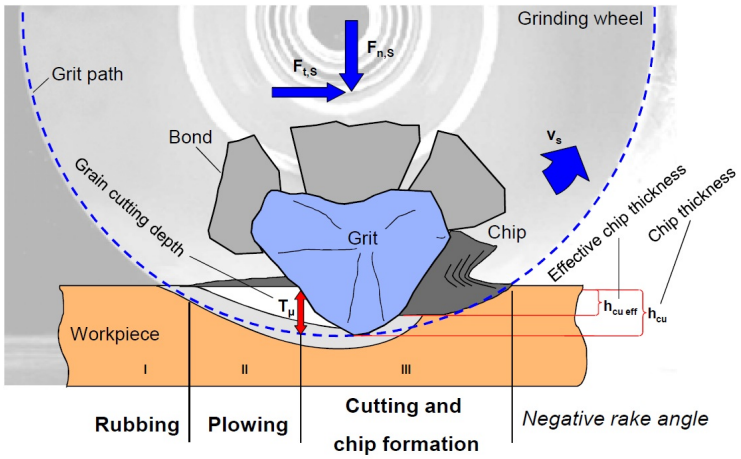

Figure 2.3: An image showing how a piece of grit removes a chip from the workpiece. The three phases rubbing, plowing and cutting explained in the text are marked. Note that the curvature of the grit's path is greatly exaggerated. *Picture: Klocke, F., Manufacturing Process 2: Grinding, Honing, Lapping, Springer-Verlag Heidelberg, 2009*

The forces created during grinding of course also affects the grits and creates wear. Pieces of or whole grits might fall off, the tips might flatten, or the pores between the grits might clog with chips. If the grits break and minute pieces fall off then the newly created edges make cutting easier and the grinding wheel effectively sharpens itself. This is a desired effect. Sharper grits require smaller grinding forces to cut the material because it is the pressure on the surface that has to reach a critical level for the workpiece to start to plasticize, and a smaller grit tip area results in a smaller normal force for a given pressure. However, should whole grits fall off then that is a sign that the grinding forces are too

large. Flattened tips on the grits and chips clogging the pores both reduce the cutting performance because the effective tip area increases, resulting in higher friction and more heat entering the workpiece.

2.2.1 Grinding burns

The energy put into the grinding process eventually dissolves as heat, transferred either to the chip (q_{chip}), grit (q_s), cooling fluid (q_{kss}) or to the workpiece (q_w) as shown in figure 2.4). Processes that generate much of the heat is the rubbing, and later the breaking of bonds in and deformation of the material. If the pores in the bonding matrix are clogged by chips then the inflow of cooling fluid is hindered and less heat is drained. If the surface of th workpiece is heated above the tempering temperature, either because too much heat is generated or because too little dissipates in other ways, thermal damage is inflicted on the surface. First the surface is softened as the heat anneals the material. This is a kind of thermal damage called *grinding burn*. If enough heat is created the surface might even reaustenitizise, and the subsequent quenching by the cooling fluid creates a very hard and brittle martensitic surface layer which is prone to cracking. That is considered a severe grinding burn.

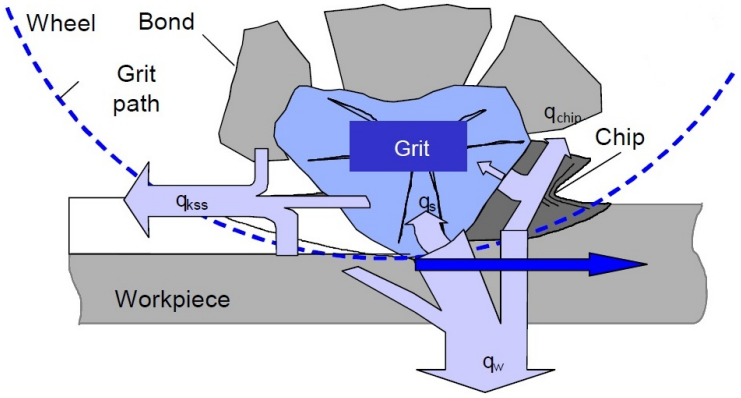

Figure 2.4: The various ways heat is transferred in grinding. The heat flow into the workpiece, q_w, is undesirable and may cause grinding burns. *Picture: Klocke, F., Manufacturing Process 2: Grinding, Honing, Lapping, Springer-Verlag Heidelberg, 2009*

2.3 Magnetism inside materials and the Barkhausen effect

The Barkhausen effect is a magnetic phenomenon that arises in the presence of a varying external magnetic field. It is related to the discontinuous waxing and waning of small magnetic domains inside the material, which will be described in the following subsections.

2.3.1 Magnetostatics

The source for the following subsection is the book "Electronic Properties of Materials" by Hummel.[5]

Magnetism is due to two phenomena: the orbiting of valence electrons around the atoms' cores and the spins of the individual electrons. These rotating charges create minute magnetic fields pointing in the directions of the rotation axes. Normally the magnetic

moments created are randomly oriented which means that the individual magnetic fields cancel each other even on a microscopic scale. Applying an external field will however re-orient and align the magnetic moments so that they either oppose or amplify the external field depending on the substance, but usually only with a small amount. In most solids only spin magnetism is observed because the electron orbits are coupled to the lattice and thus cannot change with the external field.

In ferromagnetic solids (e.g. ferritic steel) the spins interact in such a way that they tend to align parallel to each other regardless of any external fields, thus creating a permanent local net magnetization. The preferred direction of alignment is along the metal's *magnetic easy axis*, the direction along which the magnetization requires the least energy. The existence of an easy axis is due to magnetic anisotropies caused by e.g. crystal anisotropy or the shape of the piece, and is a prerequisite for ferromagnetism. If left alone this mechanism would align all spins in a piece of material. However, that would result in the generation of a field outside the material which costs magnetostatic energy. To reduce this energy the magnetization splits up into domains (see figure 2.5), and eventually an optimal domain size balances the two mechanisms. The domains are generally ordered along the grains' magnetic easy axis with adjacent domains rotated 180 degrees, and 90 degree domains near the grain boundaries (see figure 2.6). As the grains are randomly oriented the macroscopic magnetization is still zero.

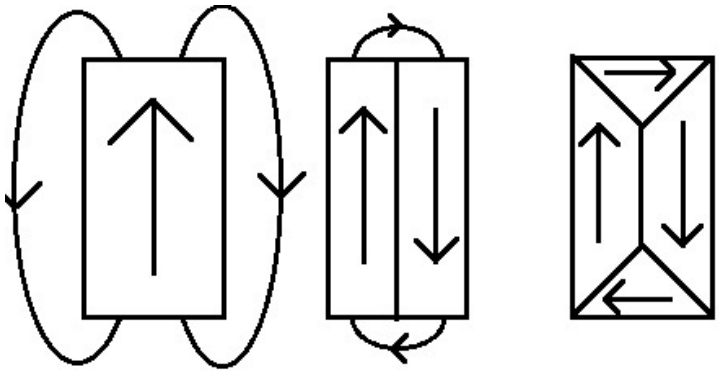

Figure 2.5: A schematic description of how domains reduce the magnetostatic energy in a simple rectangular piece of material. The original single domain is split into two smaller domains rotated 180^o from each other. For each splitting of domains the size and strength of the outside leakage field is reduced, until in the final picture no leakage field is needed to form a closed magnetic loop.[5]

These domains are separated by thin walls – areas where the orientation of the magnetic moment gradually changes to match the adjacent domain. Without external fields the domains are usually 1-100μm and the walls are measured in tens of nanometers.

2.3.2 Magnetodynamics and the Barkhausen effect

The response of a ferromagnetic material to an external field H is shown in figure 2.7. As the external field is slowly increased from zero the material will exhibit a magnetization that rises with the external field until saturation, M_s. Decreasing the field to zero again after the piece has been magnetized to saturation will leave a considerable magnetization M_r, called *remanence*. In order to restore the original magnetization of zero a field in

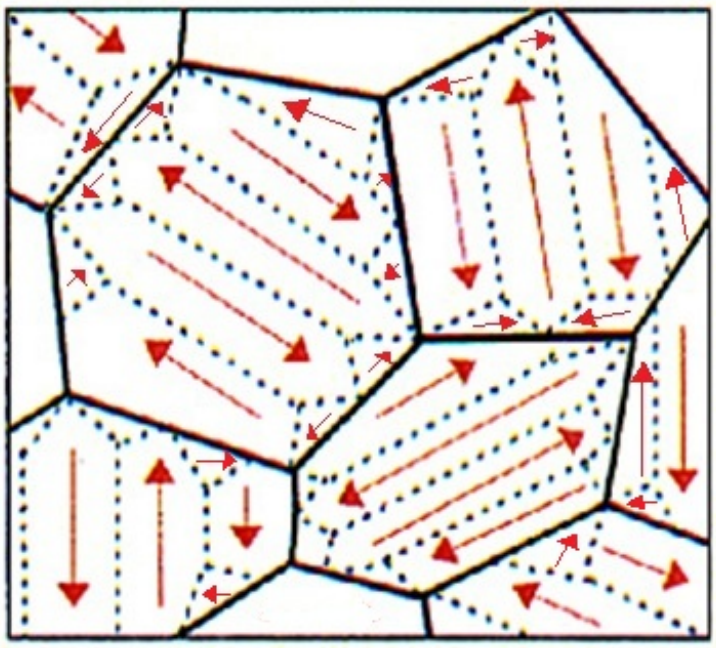

Figure 2.6: Domains in a polycrystalline material. Each grain's main domains are oriented along that grain's easy axis, such that the net magnetization of the material is zero. *Picture: Stresstech Oy.*

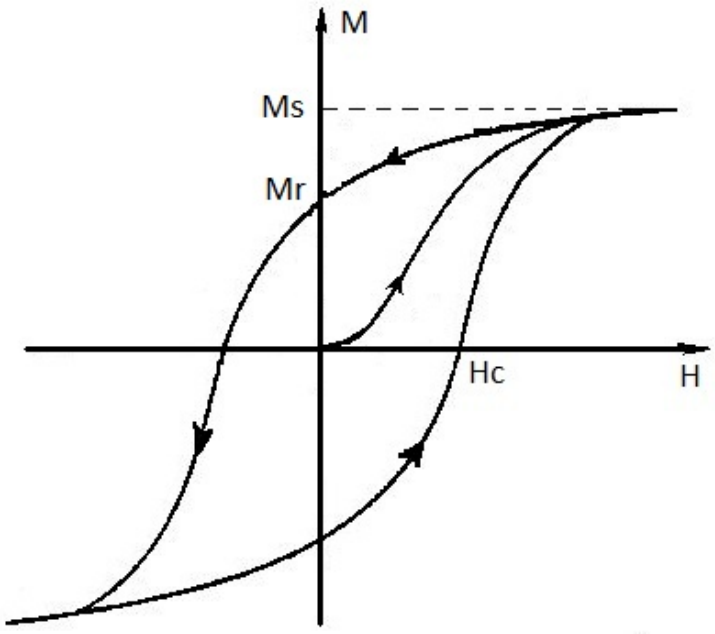

Figure 2.7: A typical magnetization curve of a ferromagnetic material. Note the hysteresis. *Picture: Wikimedia Commons.*

the opposite direction needs to be applied, H_c. The strength of this field is called the *coercivity*. This causes hysteresis in the material's magnetization curve. Large remanence and coercivity give a large hysteresis loop and a material that is reluctant to changing its magnetization, e.g. permanent magnets. Such materials have a high *magnetic hardness*.[5]

On the microscopic scale this behavior is due to the dynamic of the domains and domain walls. Applying an external field on an ferromagnetic material does not cause all spins in the material to gradually turn towards the direction of the field, but rather that the favorably aligned domains grows at the other domains' expense. This growth is not continuous, but the walls' motion is hindered by dislocations, grain boundaries, stress fields etc.[6;7;8] They pin the wall until the field is high enough to force the wall past the defect, and then the wall quickly expands until it encounters the next obstacle. The presence of hysteresis at all is also due to the pinning of domain walls; without an external field in the opposite direction there is nothing that forces the walls past the last obstacles, thus giving the remanence. The result is that whole areas inside the material changes magnetization simultaneously, and the magnetization curve is really a series of small steps. Indeed a close examination of the hysteresis curves always reveals stepwise changes. The Barkhausen effect is precisely this, the fact that the change in magnetization is discrete.[5]

2.3.3 Using Barkhausen noise as a grinding burn measurement method

Placing a coil close to the sample enables one to detect the changes in magnetization caused by the external field. The sharp steps in magnetization causes bursts of voltage in the coil which, if the coil is then connected to a loudspeaker, can be heard as clicks or a buzzing noise (see figure 2.8). This is the origin of the term Barkhausen noise.

The shape of the voltage signal is extremely sensitive to the sample's state regarding chemical composition, microstructure, hardness, surface stresses etc. while still being repeatable. Small differences due to different initial states or thermal effects exist, but their magnitude is negligible compared even to the background instrumental noise.[9] The theory describing the effect of changes in the mentioned material parameters on the signal is still largely unknown and an area of research itself.[10;11] A short review of the most prominent theoretical descriptions will be given below, after which a summary of conclusions from more phenomenological studies directly related to this thesis will be given.

The notion of using the Barkhausen effect as a non-destructive test method for metals was developed in the early 70's. Early studies on the applicability of the technique were performed by Tiitto[12;13;14] during the rest of that decade. Several other attempts to find mathematical relationships between material properties and the Barkhausen response followed, but no theory describing the dynamics of the domain wall motion was formulated until Alessandro et al. presented their model in 1990.[15] This would henceforth be known as the ABBM model. This model was developed for systems with one domain wall but can be extended to systems with many walls. It is based around the hypothesis that the pinning field, that is the field through which the wall moves and which determines its speed, is a random walk in space. It successfully describes the power spectrum of the Barkhausen signals, but gives no microscopic justification of why the random walk hypothesis is a reasonable hypothesis. In 1998, Zapperi and Cizeau presented another model called the CZDE model.[9] It describes a single domain wall using the theory for flexible walls driven through disordered media. Interestingly they find that the CZDE model reduces to the ABBM model under certain restrictions. Further it, among other things, predicts the avalanche like noise bursts that are characteristic for the Barkhausen effect. It however does not

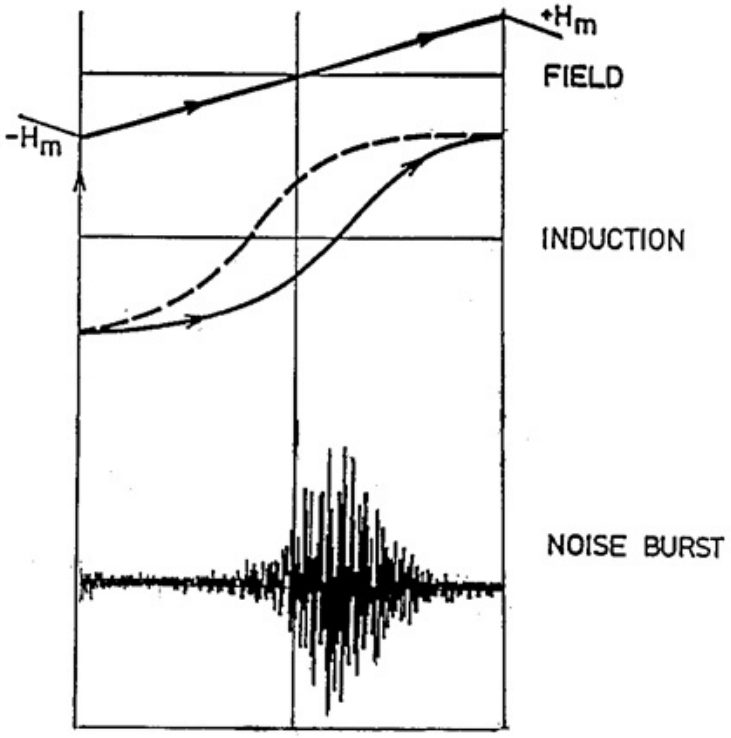

Figure 2.8: Graph showing the applied external field (top), the resulting magnetization in the material (middle), and the recorded Barkhausen noise burst (bottom). *Picture: Stresstech Oy.*

relate any signal features to microscopic material features such as grain size or residual stresses.

Studies that relate the variations in Barkhausen signals with material properties are therefore purely phenomenological. Early attempts were performed by Kameda and Ranjan in 1986 resulting in two articles. The first[6] relates the Barkhausen peak voltages to carbon content and hardness, and the second[7] the effect of intergranular impurity segregations. Further they correlate their result to a model based on the mean free path of the domain wall along with the nucleation and annihilation of small domains. Soon it however became apparent that the individual influence of different microstructural parameters on the Barkhausen response was not easily deduced, and indeed all relationships are still not well established[16]. For example the effect of dislocations, grain size, phases and carbide precipitates can be found in literature but the effect of carbon content is still disputed[16]. To complicate things further the effect of changing two parameters A and B simultaneously is not a superposition of the individual changes of each of the parameters[17]. Generally, though, the BNA tends to increase with smaller grains because there are more active walls. Dislocations, alloying elements in solid solution and small precipitates increase the number of jumps and duration of the signal, but usually lower the amplitude of each burst. This is because the amplitude of the signal is related to the speed of the Bloch wall and many finely dispersed impurities hinder the wall motion. Larger precipitates pin the walls hard and yield fewer Barkhausen jumps but each pulse is often stronger. The phase of the particular precipitate can however make great difference for the end effect on the BNA[17;6].

Because the Barkhausen method is so sensitive and the effects of so many material pa-

rameters are unknown it is usually impossible to compare the BNA for different materials, but a reference needs to be produced for each application. Also the response varies with the amplitude and frequency of the external field. Still it has been proven that the Barkhausen method could be used to detect grinding burns.[2;3] Grinding burns affect several of the parameters mentioned in the beginning of this chapter; most importantly surface hardness and retained austenite levels are reduced due to tempering, and residual stresses are moved towards tension. All of these changes increases BNA and grinding burns are therefore easy to detect.[2;3] Also, the BNA measure is a result of a quite shallow sampling depth, which makes the method suitable to asses surface changes such as grinding burns. Tests at Scania have established some relationships between various parameters and recorded BNA for the specific material used in crankshafts, and proven that grinding burns can be detected.[18] These results will be presented in chapter 2.4.

2.3.4 Barkhausen Noise measurement method

The Barkhausen noise (BN) is measured with a special machine that both creates the external magnetic field and detects the sample's magnetization. A schematic image of the design is shown in figure 2.9. One magnet produces the external field and a pick up coil located in between measures the induced magnetization. The external field forces the sample through (at least) one lap in the hysteresis curve at every point of measuring and the signal is recorded. Every lap creates two bursts of noise: one when the material is magnetized in one direction and another when the magnetization is inverted. The measurement depth for these bursts is measured in tens of μm according to Stresstech. For each burst the root mean square of the signal is calculated, and the resulting number is called the BNA or Barkhausen Noise Amplitude. The acceptance levels at Scania are empirically set by comparing to strength requirements, and the shaft is discarded if any measurement is above the acceptance level.

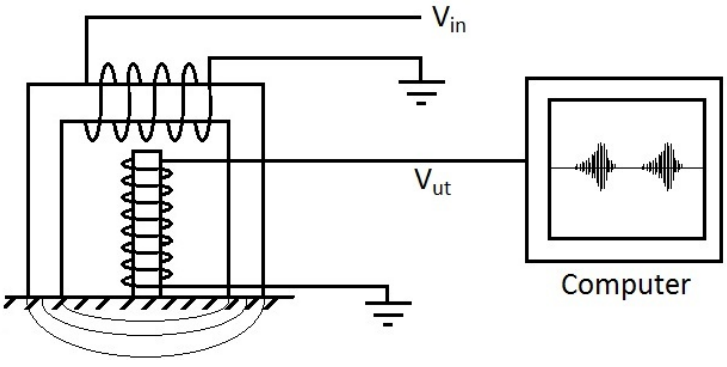

Figure 2.9: A schematic of a Barkhausen analysis apparatus. The horseshoe-shaped electromagnet produces the external field and the the smaller metal bar and coil placed in between picks up the magnetization on the surface. The external field is alternated by varying the voltage V_{in} and the BNA is calculated from the output signal V_{out}.

2.4 Previous studies at Scania

A number of related studies[19;18] have preceded this one at Scania, the results of which have served as input to this thesis. All references for this section will thus be to internal

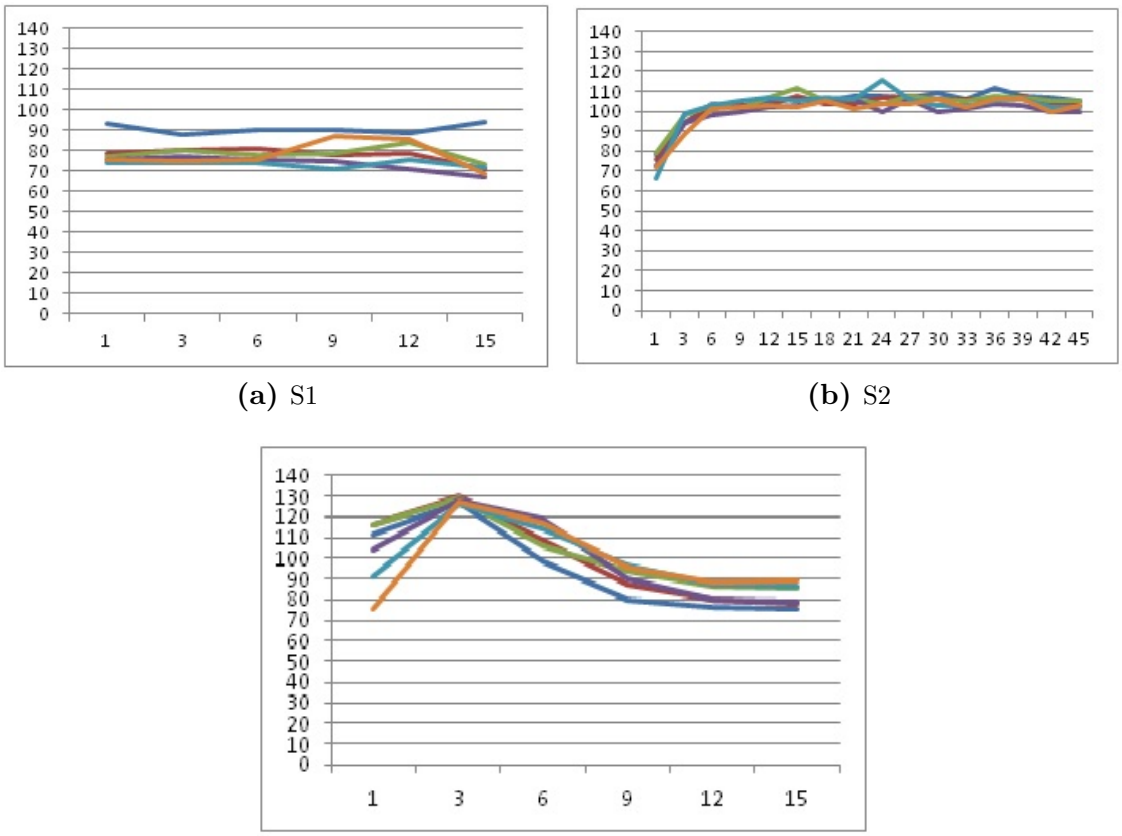

(a) S1

(b) S2

(c) S2 followed by S1

Figure 2.10: Results from grinding tests performed at Scania during the winter of 2011. The x-axis counts number of crankshafts after the last dressing and the y-axis displays the maximum BNA for each of the six crank bearings.

reports at Scania. The problem with varying BNA levels dates back several years and has complicated the development of an industrialized control method of crankshafts. The start of this thesis was the discovery in the summer of 2011 that the Barkhausen levels not only vary between batches and different compositions, but also between suppliers.

Grinding tests (see figure 2.10) show that supplier S1's maximum BNA lies steady at around 75-80 for crankshaft after crankshaft after the last dressing of the grinding wheel. Supplier S2's crankshafts start with BNA values around 75 for the first crankshaft grinded after the last dressing, but the BNA value slowly rises to a steady state between at 100-110 after 7-10 crankshafts. It is common for grinding processes to exhibit a rising transient if you plot grinding force versus time, as dulling grits increase the grinding forces (see section 2.2), and increasing force means more heat, greater likelihood for grinding burns and higher BNA. The lack of transients in measurements for the crankshafts from S1 could then be because the grinding wheel sharpens itself immediately. Thus, the only remarkable point was thought to be the distinctively different steady state levels. However, when crankshafts from S1 in one test was grinded after crankshafts from S2 without dressing in between a sinking transient could be seen. Grinding processes generally do not exhibit sinking transients.

If the differences in BNA were only due to different materials then the change in BNA

should be abrupt. The transients show that there is a history in the grinding wheels. This in its turn implies that the difference in BNA originates from the interaction between the wheel and the crankshaft. Different ways to examine this have been tested, but before the start of this thesis project they were all inconclusive. Most notably a small piece of grinding wheel has been examined in a scanning electron microscope but the images were blurred because of charge build up.

2.4.1 Parallel studies at Scania

During the execution of this thesis project parallel studies were conducted at Scania, and they were used to support conclusions drawn in this thesis study. Therefore the core results of these parallel studies will be presented below. Thus, note that these results were not known at the start of this thesis project.

In a report released on January 31st 2012[18] the relationship between BNA, residual stresses, hardness and grinding burns detected through etching on the washers of Scania's crankshafts was examined. In this report it is stated that the hardness falls below the lower specified limit when the BNA exceeds 110. The residual stresses change to tensile at a BNA of 90 and grinding burns become visible after etching for a BNA of 100 or higher. The results are shown in figure 2.11 and they will be used as reference for the hardness and residual stress tests performed within this thesis study.

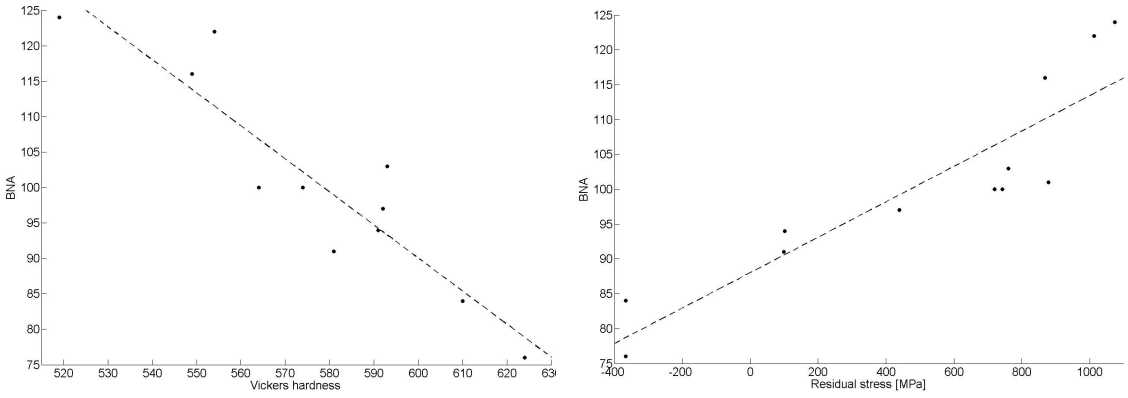

(a) BNA vs surface hardness. 1kg weight measured 0.1mm below the surface.

(b) BNA vs maximum residual stress

Figure 2.11: Results from hardness and residual stress tests in Jan 2012.

In early April 2012, during the third phase of this diploma thesis study when the various test bars were being manufactured but no actual test had been performed, the production unit at Scania presented some preliminary results from an on-going study by Dr. Krajnik at KTH. In the study a series of grinding tests were performed among which one is of particular interest for this study. Because these tests are part of an yet unpublished article the actual results will not be presented here, but a summary of the main results important for this study will be given below.

This test concerned the truing and dressing of the grinding wheels and consisted of grinding series where the wheel was dressed in a manner as to mimic the effect of varying degrees of chips clogging the pores. Then the energy consumption of the wheels was

measured over time. The results showed that roughly 10% more energy was consumed during grinding of the crankshafts from S2 compared to those from S1. This difference remained through all of the test series with the exception for the most clogged grinding wheel. The implications these results for this thesis are discussed in section 5.4 after presenting the results of my thesis study.

3 Crankshafts

An image of a crankshaft is shown in figure 3.1. The crankshaft transforms the force from the pistons into a torque in the engine's outgoing axle. The crank bearings are located on the off-centered parts of the shaft and this is where the connecting rod is mounted. This is the area that is most sensitive to cracking and mishaps in the grinding procedure, and thus it is also the area inspected with the Barkhausen method. The main bearings holds the crankshaft in place inside the engine block and the counterweights reduce vibrations.

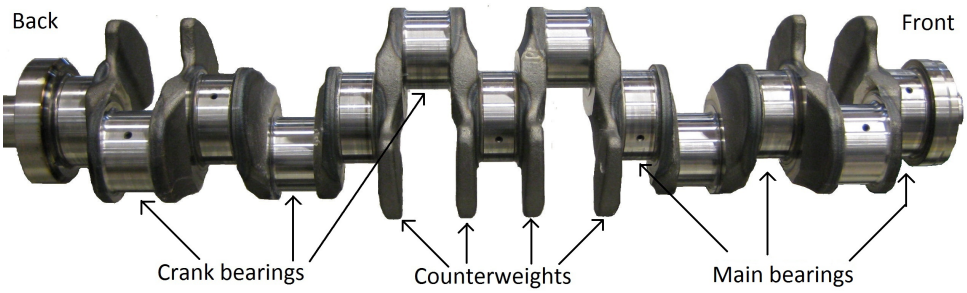

Figure 3.1: One of the crankshafts used in the present study.

The material used in the crankshafts is a slightly modified version of so-called C38 steel with nominal carbon content range of 0.35-0.40%. The used material is a precipitation hardening pearlitic/ferritic low-alloy steel which is delivered in forged condition. Two suppliers called S1 and S2 are compared in this thesis. Supplier S1 forges the crankshaft from ingot cast steel made from ore, while supplier S2 uses continuous cast steel made from scrap metal. At Scania the part is then soft machined, induction hardened, tempered and ground into the finished crankshaft. The manufacturing at Scania is identical regardless of supplier.

For this thesis 5 crankshafts were examined, henceforth labeled A-E, of which A-C are from supplier S1 and D-E are from supplier S2. Of the crankshafts from S1, A is from a separate steel charge. The chemical composition of each crankshaft together with the specified composition is presented in table 3.1. The mechanical properties are presented in table 3.2. Data are according to material certificates issued by the suppliers.

Table 3.1: Chemical composition of Scania's crankshafts according to suppliers' certificates. Numbers marked with an asterisk were missing from the certificates and were measured at Scania using Glow Discharge Optical Emission Spectroscopy.

Element	Specified content	A	B, C	D, E
C %	0.35 - 0.40	0.38	0.38	0.36
Si %	0.45 - 0.65	0.51	0.50	0.55
Mn %	1.30 - 1.50	1.37	1.38	1.32
P %	<0.025	0.014	0.010	0.008
S %	0.018 - 0.033	0.024	0.024	0.021
Cr %	0.20 - 0.30	0.23	0.23	0.22
V %	0.08 - 0.12	0.095*	0.093*	0.10
Al %	0.005 - 0.030	0.020	0.021	0.011
Cu %	<0.35	0.24	0.20	0.30
N %	0.0090 - 0.0200	0.0115	0.0108	0.0103
O pp	<20	4	6	16
H ppm	<2.0	2.0	1.0	1.0

Table 3.2: Mechanical properties according to suppliers' certificates

Property	Specified	A	B, C	D, E
Grain size (ASTM)	>3	6	4	5
Yield stress	>550	558	578	591
Tensile strength	850 - 1000	840	884	877
Elongation %	>12	13.2	12.5	15.5
Area reduction %	>25	22.8	25	40
Hardness	250 - 300	265	265	260

4 Part 1: Barkhausen Noise measurements and hysteresis curves

4.1 Barkhausen Noise measurements

Before any other tests and analyses a BN measurement was done. The purpose of this was to obtain reference curves with which areas of interest for further investigation could be chosen. The first set of investigations thereafter would include microstructure analysis, residual stress measurement and assessment of hardness profiles. The BNA curves would therefore be examined for points that were believed to yield relevant results for these methods.

For this measurement a Rollscan set-up from Stresstech was used, as it was the equipment available. A picture of this experimental set up is seen in figure 4.1. The BNA was recorded at approximately 145 points evenly distributed over one lap around the crank bearing, the data forming one BNA curve. Curves were compiled for the washer, radius and bearing on both sides, forming a total of six curves for each of the six crank bearings for each crankshaft (see figure 4.2). Every measurement was repeated twice, and only accepted if both laps gave identical curves. The average of these curves for the washers were compared with previous measurements from the production unit before they were approved, in case handling errors had occurred.

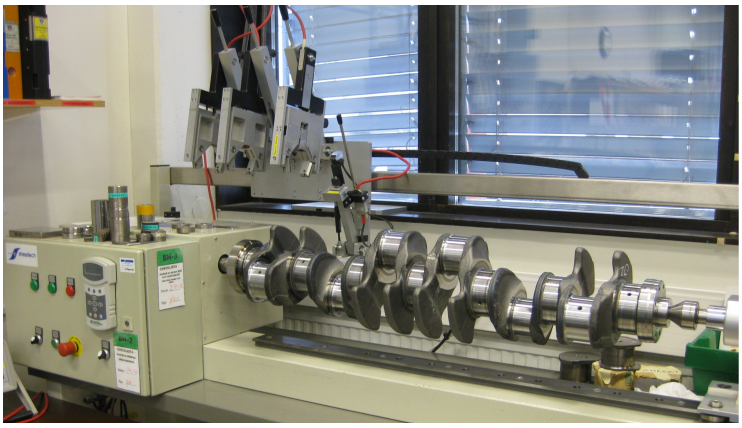

Figure 4.1: Experimental set up for the Barkhausen Noise measurement. The shaft is rotated so the sensors can measure the BNA around the bearing. The three sensors for the bearing, radius and washer are seen on top.

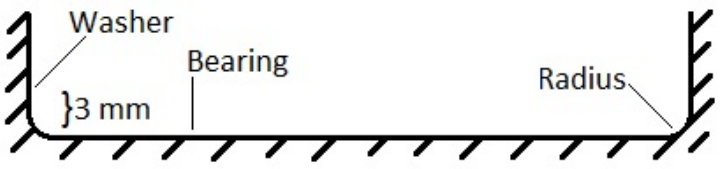

Figure 4.2: Cross section of the bearing on a crank. The washer curves are measured 3mm above the bearing surface. The bearing curves are measured over a wider section 0.5-1 cm in from the washers.

4.1.1 Results

The BNA graphs obtained can be found in figures A.1-A.5 in appendix A, and one typical example is shown in figure 4.3. Several characteristic features can be found on the radius and bearing graphs. The crankshafts from S1 have a lower amplitude on their BNA and all of the crankshafts from S1 are more uneven than their S2 counterparts. The radius always has a considerably lower amplitude than the bearing and washer because the difficulty in positioning the instrument at the surface in the inward bend.

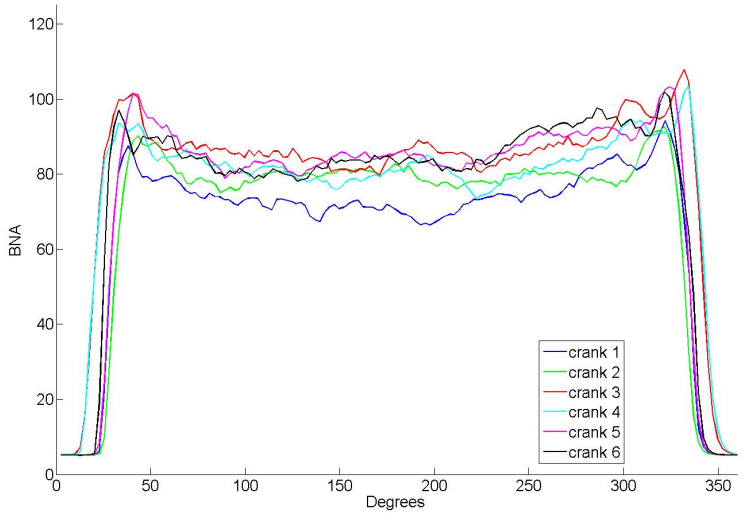

Figure 4.3: Example of a BN curve, this one from the front washer of crankshaft B.

When examining the washers' graphs a few other distinct features are revealed. Firstly we see that the most typical feature is the drop to BNA value of 5 at the ends of the curves. This is because the washer only covers a certain portion of the lap, and thus the BNA is measured in air elsewhere. Secondly the BNA almost always overshoots at the transition between washer and air. Thirdly the BNA dips in the middle on the crankshafts from S1 whereas the ones from S2 are fairly constant throughout the lap, and the average is higher for the crankshafts from S2. Lastly front graphs are always more even than the back washers'. This is a known problem; the back washers are more difficult to grind.

One possible source of errors is handling errors, but several steps were taken to minimize this effect. As the method is very sensitive to dirt on the surface and the distance between detector and surface, this could have a large impact on the BNA. However it is unlikely that the same handling errors would occur during several measurements and by different operators, and thus this effect should be small.

4.2 Hysteresis curves

Examining the magnetic properties of the materials could assess the possibility that the difference in BNA would come from a difference in said magnetic properties. The method chosen was to plot and compare the hysteresis curve for each material. The reason for this choice of method was that it could be done in no time with the existing Barkhausen hardware. Also the hysteresis curve yields many important magnetic parameters: permeability, coercivity, remanence and saturation (see subsection 2.3.2). Finally the shape itself of the curve yields information on the material's response to varying external fields. A downside

with using the BN equipment is that it does not, in fact, measure the actual magnetization but calculates the hysteresis curve from the same signal as the Barkhausen noise. Any errors this might lead to was however expected to be equal for all crankshafts.

The measurements were executed on the fourth crank of each crankshaft except for crankshaft E where the measurement was executed on crank six. The reason for this was that there were no pieces left of the fourth crank on crankshaft E, they were being worked into test specimen for the following experiments. For each crankshaft four complete hysteresis curves were plotted; axial and radial/tangential direction of the external field both in the bulk and on the bearing surface. Axial direction is parallel to the shaft axis and radial/tangential perpendicular to this axis.

4.2.1 Results and discussion

The measured hysteresis curves are shown in figures 4.4-4.5. In figure 4.4 the curves obtained from the bulk material are shown, and we see that there is generally no differences between the crankshafts or between the axial and radial direction (the one different curve will be discussed below). This is not the case in figure 4.5 where the curves obtained on the surfaces are shown. Although there is no difference between different crankshafts there is a huge difference depending on direction. This is because the grinding is acting on the surface in only one direction and this has a huge impact on the residual stresses, which in its turn affects the magnetic response (see subsection 2.3.3).

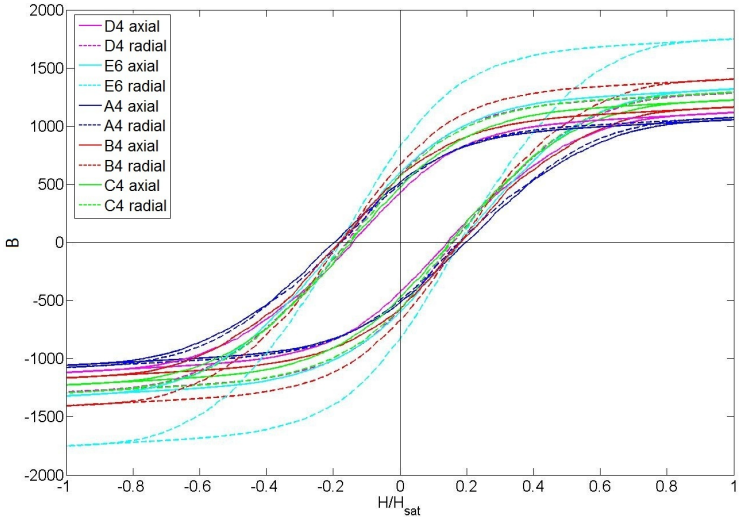

Figure 4.4: Hysteresis curves measured in the bulk material on the cranks. Axial direction is when the external field is aligned along the axis of the shaft, and for radial direction the external field is directed perpendicular to the shaft's axis.

The differing curve in figure 4.4 is measured on specimen E6 in radial direction. From the figure we see that the coercivity is the same as those of the others but the remanence, saturation and energy consumed forcing the material through one lap in the hysteresis curve is different. Also the permeability is slightly higher. The difference could be caused by the sawing process used for exposing the bulk inflicting some kind of stresses or heat, but it could also be caused by local magnetic anisotropy. Some anisotropy is evident in all crankshafts, due to the way the material is deformed during forging, and possibly this effect is more prominent on some cranks than on others because of the manufacturing.

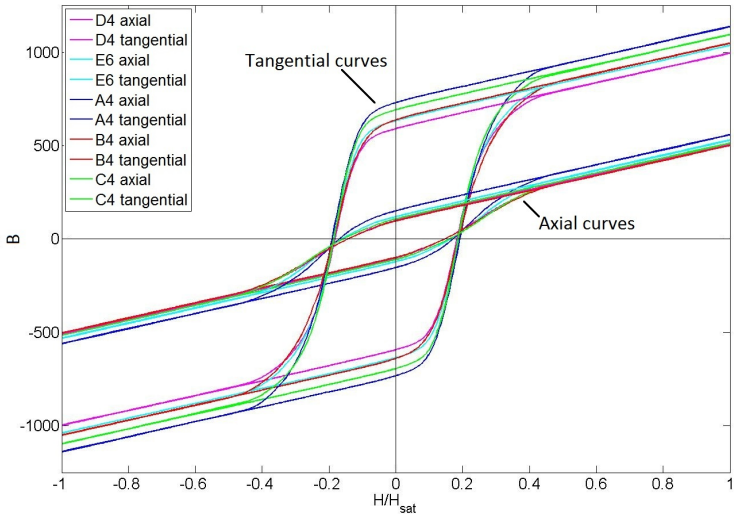

Figure 4.5: Hysteresis curves measured on the bearing surface on the cranks. Axial direction is when the external field is aligned along the axis of the shaft, and for the perpendicular tangential direction the external field is directed along a tangent to the rounded bearing surface.

4.3 Discussion and summary of part 1

The second set of experiments done after part 1 comprises hardness testing, residual stress measurement and microstructure analysis. As stated in section 4.1, the location of these tests would have to be determined from the BN curves. Since the hysteresis curves were similar for all crankshafts no consideration would have to be given to the local magnetic properties when choosing from these curves. It was decided that the specimens would primarily be taken from the front side unless there was something of specific interest on a back side, as the purpose of the following studies would be to examine the material itself. Choosing from the back side would mean an increased possibility that the BNA would be caused by variations in grinding procedure rather than in material properties. This could have been a more suitable choice had the purpose been to improve the grinding process. Also the locations would be decided from the washer curves only as the other curves were relatively constant throughout the entire circumference.

From the results of the BN measurement it was decided that specimens for the hardness and microstructure examinations would be taken from the front side of the fourth crank on each crankshaft, approximately 180 degrees from where the washer curves measure in air. The reason for this choice was that the fourth curve was usually close to the average of the other curves, and the farthest side from the disappearing washer is least likely to be affected by the overshoots. Identical specimens would be taken from the front side of the sixth crank on crankshaft E to examine the large variation in BNA within that crankshaft. Also two specimens would be taken from the back side of the first crank on crankshaft D to examine the strange variation in BNA within that washer. On all of these specimens hardness profiles would be produced for both washer, radius and bearing and the microstructure would be examined at these surface locations.

Residual stress would not be examined at all of these locations as it is a time consuming procedure. A specimen for this would be taken from crank four on crankshaft B as close to the hardness specimen as possible, and this would represent the crankshafts from S1. Two more would be taken from cranks four and six on crankshaft E close to the hardness

specimens there, the fourth representing the crankshafts from S2 and the sixth examining the unusually low BNA. Another two would be taken from the first crank of crankshaft D, near the hardness specimen, to examine the same variation in BNA on that washer.

All specimens are marked in figures A.1-A.5. The BNA for these locations are listed in table 4.1 and are approximate because of the difficulties in picking a specimen from an exact part of the curve. They should however not differ more than a few units as each specimen as far as possible represents relatively constant parts of the BNA curves, and it is not believed that the BNA varies much between any of the 145 measurement points.

Table 4.1: Measured BNA at the locations examined in chapter 5

Specimen	A4f	B3b	B4f	B4b	C4f	D1b1	D1b2	D4f	E4f	E6f
BNA	70	97	80	70	105	87	110	117	92	65
Figure	A.1e	A.2f	A.2e	A.2f	A.3e	A.4f	A.4f	A.4e	A.5e	A.5e

5 Part 2: Materials testing and analysis

5.1 Hardness testing

The hardness was tested at the surface for comparison with the BNA. Also a hardness profile was constructed by measuring the hardness at different depths. The hardening depth is defined as the depth where the hardness is 400HV. Hardness profiles were taken from the washer, radius and bearing on the ten previously mentioned locations marked in figures A.1-A.5. These consist of ten indentations each, one every 0.5 mm from the surface, measured with a 10 kg weight. Also the surface hardness on the washer was measured three times with a 1 kg weight 0.1 mm below the surface. See figure 5.1 for an example.

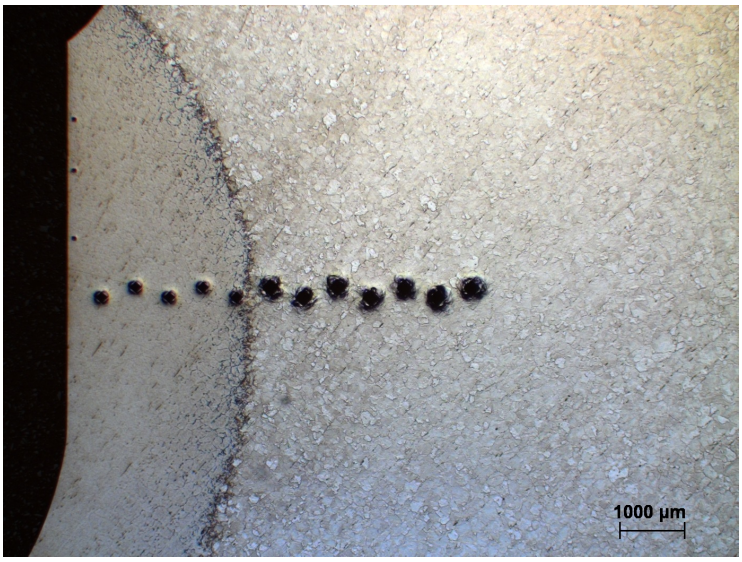

Figure 5.1: Picture showing the hardness indents on the washer of hardness sample A4f.

5.1.1 Results

The results from the measurements are presented in figure 5.2. Although the hardness profiles are similar there is still differences in surface hardness, hardening depth and bulk hardness. First of all the hardening depth is definitely largest on the bearing curves, where it is most needed. It is interesting to note that the depth profiles that do not conform with the others are the ones from locations that were chosen because the BNA was unusually high or low (dotted lines), with the exception of E6f whose low BNA will be explained by its residual stress in section 5.2. However the BN method hardly measures the Barkhausen noise as deep as the first indentation at 0.5 mm, so the hardness profiles beyond this depth is not relevant.

Plotting the average of the washer surface hardnesses received with the 1kg weight versus BNA in that point shows that the BNA decreases as the hardness increases, in agreement with previous research (compare figures 2.11a and 5.3)[18]. The relationship is even clearer when the outermost hardness value received with the 10kg weight (0.5mm below the surface) is plotted against BNA, possibly because the larger indentation tip makes the hardness measurement less sensitive to local variations in microstructure. With the exception of three measurements, the decrease in BNA is almost linear with increasing

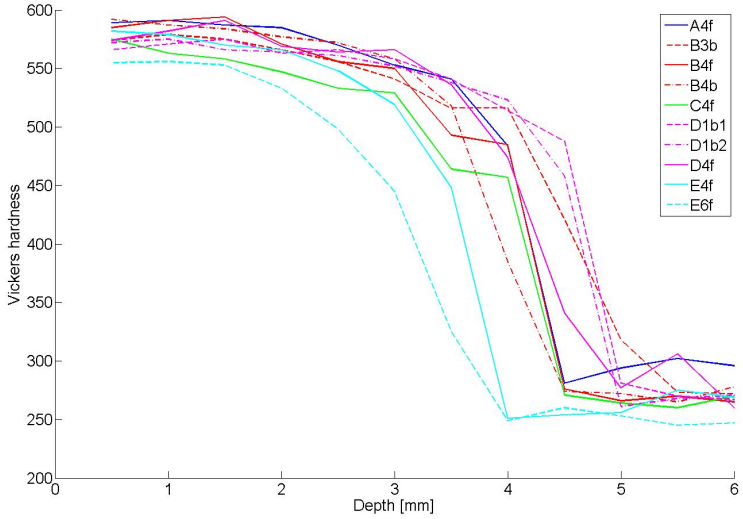

(a) Bearing

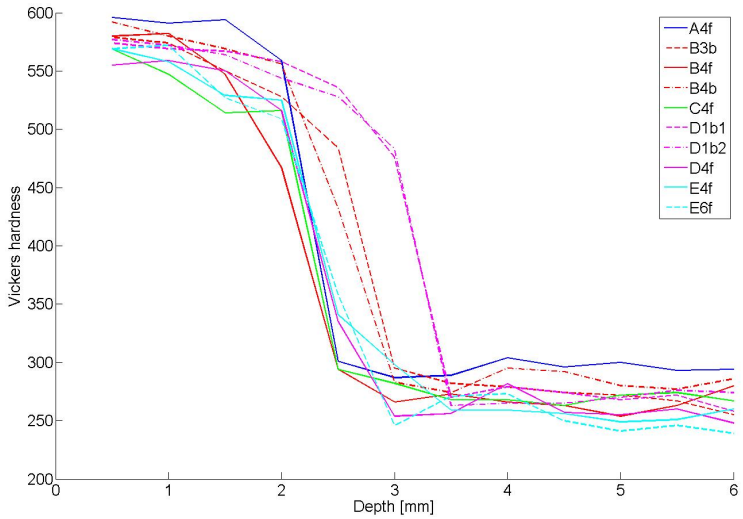

(b) Radius

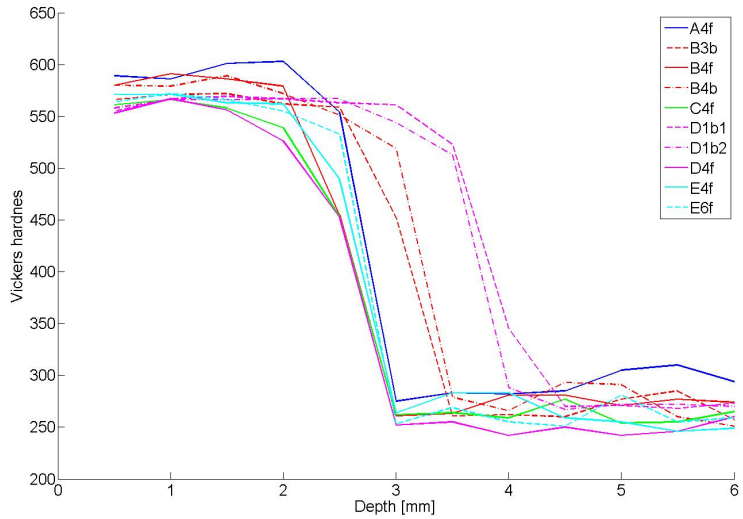

(c) Washer

Figure 5.2: Hardness profiles for the bearing, radius and washer for each of the ten samples measured with a 10kg weight.

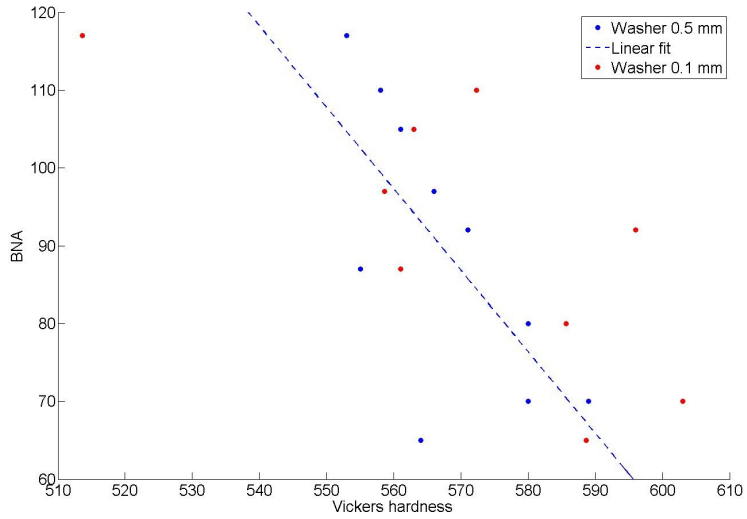

Figure 5.3: Comparison of the measured surface hardnesses versus measured BNA in that point. Both the measurements from 0.1mm and from 0.5 mm below decrease in BNA as the hardness increases, but the 0.5mm measurements are better approximated by a linear fit as their spread is less.

hardness. The three deviating measurements are D1b1, B4b and E6f, all of which showed unusually low BNA data. The most deviating one is E6f, but again the low BNA is probably due to an exceptionally compressive residual stress. D1b1 might also be explained with its residual stress, but the stresses for B4b are unknown. No other way to explain the low BNA values of these three measurements has been found. The fact that the BNA analysis depth is less than the hardness measurement depth could however be responsible for this.

Comparing BNA values to the hardening depth showed no connection whatsoever. Neither is any supplier's crankshaft's surface hardness remarkably high or low but they are evenly spread.

5.2 Residual stress measurement

The residual stress state at the surface is paramount in preventing cracks. For good fatigue strength the stresses in the surface layers need to be compressive, but heat developed during grinding drives the stresses towards tensile. This is the main reason why grinding burns increase the risk for cracking.

The residual stresses were measured using a Stresstech Xstress 3000 G3R X-ray diffractometer. It uses X-ray diffraction to measure the distance between the atomic planes based on Bragg diffraction and compares this to the stressless state, whereby the stresses on the surface can be determined using the Young's modulus and assuming elastic distortion. Depth profiles were constructed by hole etching away material between each measurement. The measurements were taken on the washers in two perpendicular directions; one radial towards the center of the crank bearing and one tangential to the bearing surface.

5.2.1 Results

The results are presented in figures 5.4-5.5. They are in good agreement with previous studies, see figure 2.11b for comparison.

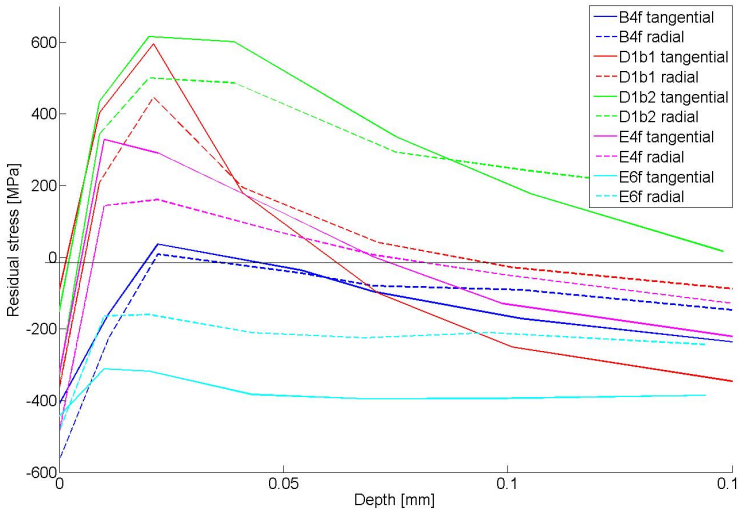

Figure 5.4: Results from the residual stress tests. The graphs show how the stresses are tensile near below the surface, due to light grinding burns, to become mostly compressive at the surface and at greater depth below the burnt areas.

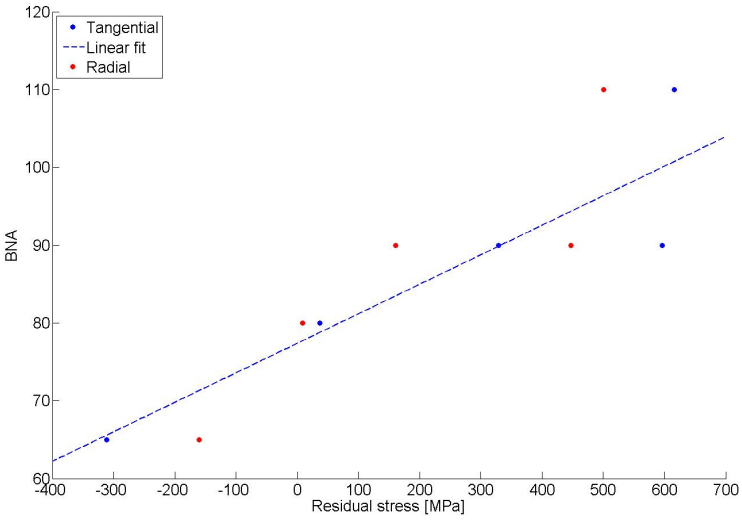

Figure 5.5: Comparison of the maximum residual stress for each specimen versus the BNA in that point. The tangential component of the residual stress, the stress component in the direction of the grinding action, scales with the BNA.

The fact that the residual stresses affect the BNA is known from theory and practice, see 2.3.3, and the strong relationship suggests that this is a major contributor to the differing BNA data in this situation. Both tangential and radial directions show that the BNA increases when the residual stresses move towards tensile, with a relationship that is nigh on perfectly linear for the first three tangential measurements. The deviations in the two last measurements, D1b1 and D1b2, can be explained if one compares the depth curves of their residual stresses (red and green). D1b1 with the unusually low BNA does have a high maximum stress, but decays rapidly and is the second most compressive curve already at 0.1mm below the surface. D1b2 on the other hand decays slowly and is the only curve still in the tensile region at 0.1mm. As the measuring depth of the BN method again is about 0.05mm there is no wonder that it has an considerable impact on the BNA. The slightly larger spread in the radial stresses is probably due to that it is perpendicular to the grinding process.

Differences in residual stress is usually credited to variations in heat generation during grinding but it could also be because the mechanical action of the grinding wheel is different. For the mechanical action to be different, however, the grinding wheels have to be different since the grinding procedure is identical. As the wheels are of identical composition, and they are dressed to identical shape and surface characteristics, any difference has to be caused by the interaction with the workpiece during grinding. Thus one conclusion from this test is that the specimens have been exposed to different temperatures during grinding, but it is also possible that some workpieces have affected the grinding wheels in some way. It is also likely that the specimens with higher BNA have been exposed to the higher temperatures.

5.3 Microstructure analysis

Two specimens with the same chemical composition could still have very different microstructure, resulting in differing mechanical properties. The magnetic behavior of metals is likewise to a large degree dependent on the structure of the magnetic medium. Thus a comparison of the microstructures of the crankshafts might shed light on their grinding performances.

The specimens used in the hardness tests were therefore etched with 2% nitric acid mixed with ethanol for approximately 5 seconds, rinsed in pure ethanol, dried with a hair dryer, and then studied with an optical microscope.

5.3.1 Results

Selected optical images of the microstructures are shown in figures 5.6-5.9.

Figures 5.6, 5.7 and 5.8 depicts the martensitic surface microstructure of the front washers on crankshafts A, B and D's fourth crank. As can be seen there is not much difference between the three specimens, and indeed any differences found between any two crankshafts were smaller than the differences between two cranks on the same shaft. Also the bulk pearlite/ferrite was similar for all specimens (see figure 5.9a).

Small variations were found in the quantity and distribution of inclusions and above all veins of bainite in the specimens. The scrap based crankshafts from S2 (D and E) contained more and coarser bainite, the largest bainite veins being several mm long (see figure 5.9b). Although the chemical composition does not differ much between the suppliers, as seen in table 3.1, both the scrap base and ingot casting could lead to a coarser distribution of

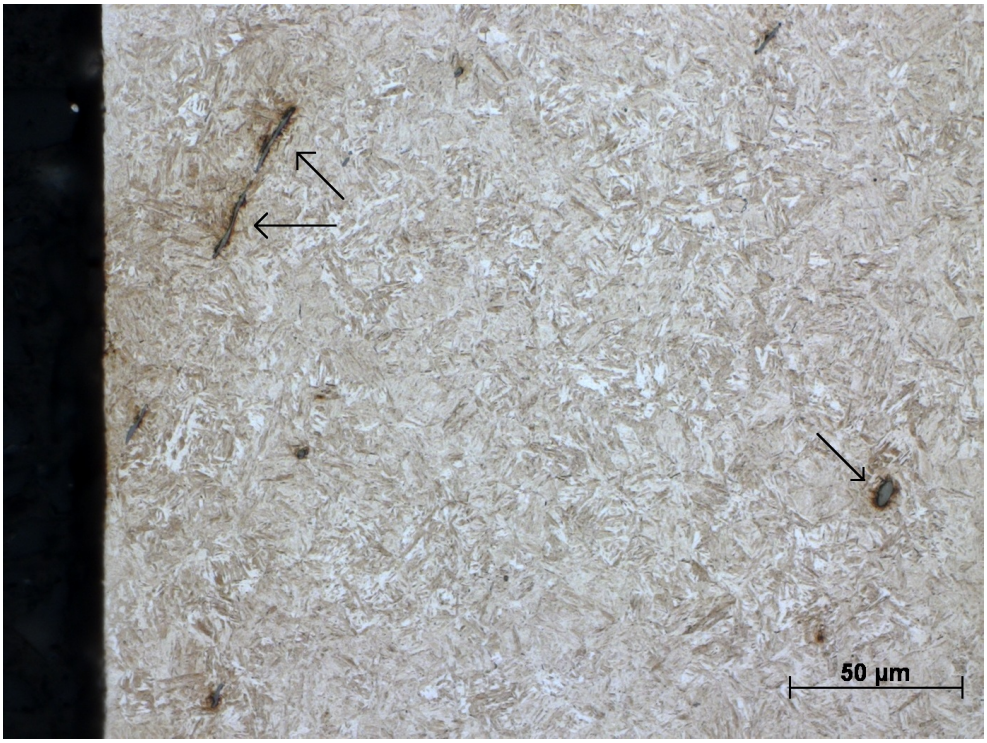

Figure 5.6: Picture of the bearing surface on A4f. The microstructure is martensitic with inclusions of MnS.

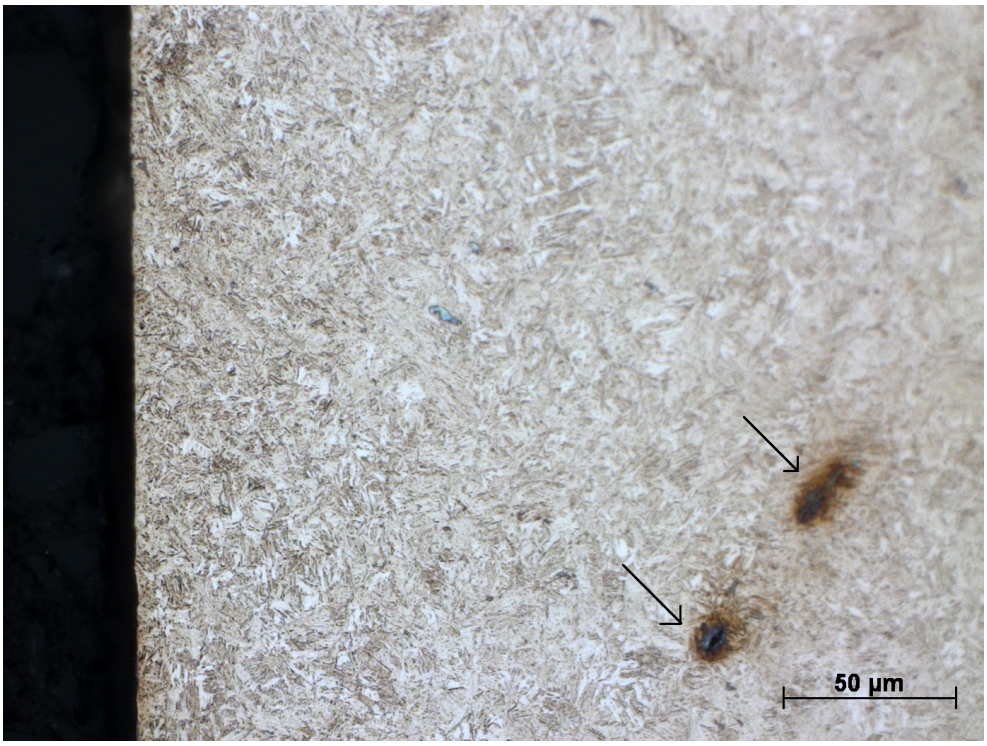

Figure 5.7: Picture of the bearing surface on B4f. The microstructure is martensitic with inclusions of MnS. The brownish areas around the inclusions are simply over etched due to nitric acid remnants in the crevices around the MnS.

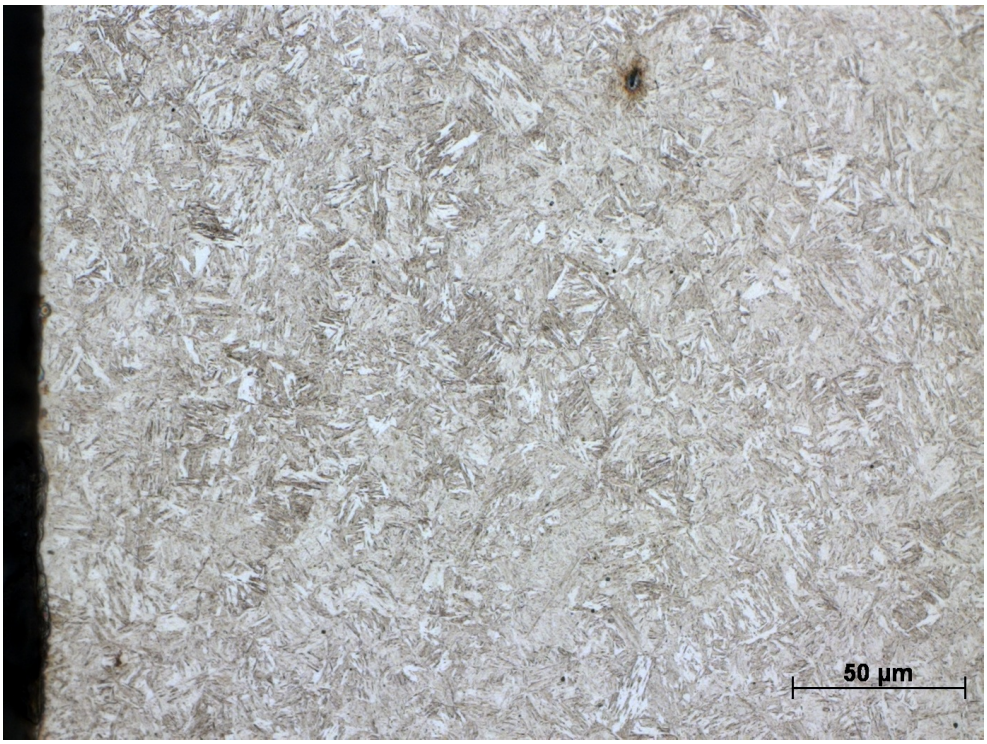

Figure 5.8: Picture of the bearing surface on D4f. The microstructure is martensitic with inclusions of MnS. The surface appears to be uneven due to some dark discoloration, probably ethanol remains.

alloying elements and impurities. Bainite can, during this manufacturing process, form if the cooling after forging is too fast and often in the presence of a high local density of alloying elements. When the bainite is part of the surface that is hardened it transforms into a kind of martensite that is distinctly different from the surrounding martensite. The microstructures resulting from bainite veins are displayed in figures 5.9c and 5.9d.

Among the specimens that contained bainite, a higher bainite concentration meant higher BNA. However, the specimens that contained no bainite gave broad range of BNA values, both high as well as low or intermediate. Furthermore the bainite veins are positioned too far below the surface to affect the BNA and are only interesting in understanding the bulk material, and the possible difference in characteristics of martensite formed. Thus the microstructure analysis showed no real differences between the materials, with the possible exception of a small difference in the homogeneity of the impurity distribution.

5.4 Discussion and summary of part 2

It is obvious from these tests that the material varies between each individual crankshaft, but generally the properties are fairly constant. The relationships found between BNA, hardness, and residual stresses agree with previous studies[18]. Furthermore the BNA correlated strongest with the residual stresses, especially the tangential stresses, as all measurements in both the hardness and residual stress tests that deviated from a linear fit could be explained by the residual stress depth profiles. No significant differences were found in the microstructures apart from some difference in the coarseness of alloying element distribution. As presented in table 3.1 the chemical composition is very similar, so thus the microstructures should be similar. The mechanical properties differed only in elongation

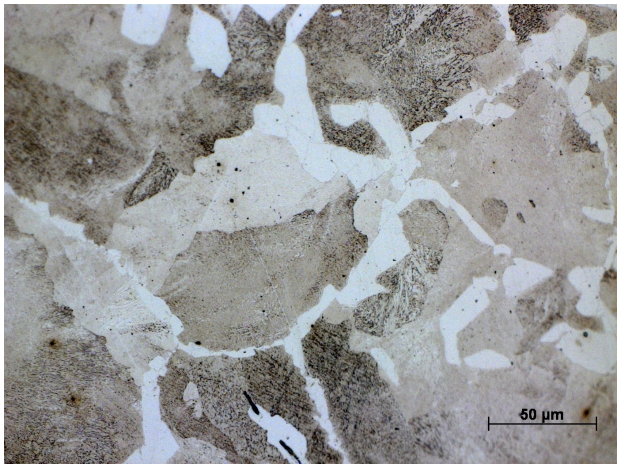

(a) Typical bulk material for all specimens, this one from E4f. The bulk is a mixture of ferrite (white) and pearlite. Minor precipitates or impurities are visible.

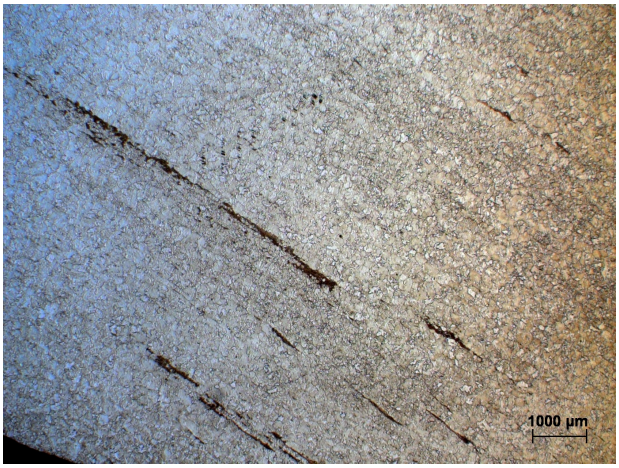

(b) Bainite veins on specimen D4f visible to the naked eye.

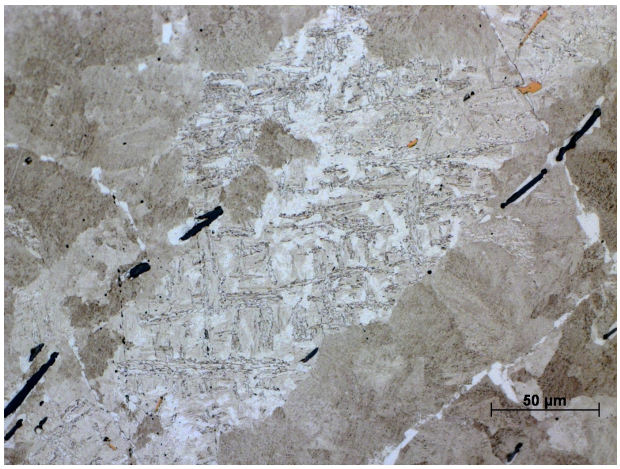

(c) A vein of bainite through the bulk pearlite/ ferrite mix in specimen A4f. The dark streaks are MnS and the yellow inclusion is TiN. Bainite is formed in areas with high alloying element concentration, which explains the high amounts of precipitates in the neighborhood.

(d) A vein of different martensite through the martensite hardened case on specimen A4f. This is the continuation of the bainite vein in (c) as it approaches the surface. Blue-grayish and yellow precipitates are still MnS and one exceptionally large TiN, respectively.

Figure 5.9: Various notable microstructural features found in the specimens.

and area reduction (see table 3.2), which shows that the bulk material of crankshafts D and E is more ductile.

The experiments during part 2 have shown that the higher the BNA, the more tensile are the residual stresses in the bearing surface. Furthermore it was deduced that the differences in residual stress between the specimen to a large extent can be credited to differences in heating during grinding. Also, the bulk material from S2, the more ductile crankshafts, shows higher BNA. Could it be that the higher ductility of crankshafts D and E means that the material in hardened condition leads to higher temperatures during grinding? If the material parameters that differed between the suppliers affected the BNA through the grinding process rather than directly, then that could help explain the transient behavior discussed in section 2.4. The hypothesis formulated is presented in figure 5.10.

Figure 5.10: The hypothetic chain of events formulated after the second experimental part.

Thus it was decided that the work would progress along two paths:

- Examine the difference in ductility further. Prove that there really is a difference in ductility. If possible, explain its cause.
  The ductility is connected to the material's ability to shear. Is it possible to see any differences in the materials' shear properties? Torsion testing is one test method that focuses on shear.
  The bulk may show a difference in ductility, but it is the hardened surface layer that is grinded. Does the ductility difference of the bulk transfer into the martensite when the crankshafts are induction hardened? To study this, tensile test with test bars of hardened material is needed.

- Fill in the gap in the hypothesis presented in figure 5.10.
  It could be that the lower ductility of S1's crankshafts causes the grinding chips to chip of in brittle fracture, which consumes less energy and generates less heat. Thus, performing a Charpy impact test can provide information about the crankshaft materials' ductile-brittle behavior.
  Also, to study grinding during the manufacturing of test pieces for the above experiments is important, especially related to heat generation and the ductility of the work piece.

The existing grinding theory has already been presented in section 2.2. There the causes for grinding burns are discussed along with the mechanisms behind grinding wheel wear. Small pieces of cutting material falling off is a good thing as this leaves sharp cutting edges and reduces the need for dressing. Too high grinding forces can, however, cause whole grits to fall off which ruins the shape of the wheel. Flattened tips and clogged pores are the last two mechanisms discussed where above all clogging is a problem connected to the grinding of softer materials.

These aspects led to the conclusion that the lower BNA and lack of transients for the crankshafts from S1 could be explained by the grinding parameters being "perfectly" matched to the application. The grinding forces were just enough that the wheel sharpens itself continuously during grinding. The crankshafts from S2, for now assuming their

greater bulk ductility does transfer to the surface and thus being too ductile for these parameters, instead start to block the pores. The heat builds up both through less cooling fluid having access to the workpiece and through gradually greater grinding forces. This explains the transient in increasing BNA found when grinding this crankshafts; the pores clog more and the forces build until a steady state is reached. The decreasing transient in BNA when switching from S2 to S1 is then explained by chips remaining in the pores for the few first grinded shafts.

The grinding tests described in subsection 2.4.1 seemed to enforce this theory. The S2 crankshafts consumed almost 10% more energy per turn of the grinding wheel, which causes more heat to enter the workpiece and which could be caused by a more ductile metal being tougher to cut. Comparing the series of tests with grinding wheels that was dressed as to simulate more or less clogged wheels shed even more light on the subject. In all of these but the most clogged one the S2 crankshafts required more energy. Hence the energy required for S2 crankshafts with non-clogged wheel matched that of S1 crankshafts with clogged wheel. The last test getting opposite results could also be explained with the ductility hypothesis; grinding a ductile crankshaft with a almost totally sealed grinding wheel would build up such high grinding forces that whole grits fall off which made the wheel deformed but clean and sharp.

Thus, the study on grinding led to the solution that possibly the material characteristics related to the ductility of the material caused more heat during grinding through the mechanism of chips clogging the pores.

6 Part 3: Dedicated mechanical tests

6.1 Torsion testing

A torsion test isolates the shear behavior of a material. A cylindrical test piece is rotated between two grips that ideally are free to slide in the axial direction so that no tensile forces are created (see figure 6.1). The ductility of a material in a grinding process relates to its shearing properties.

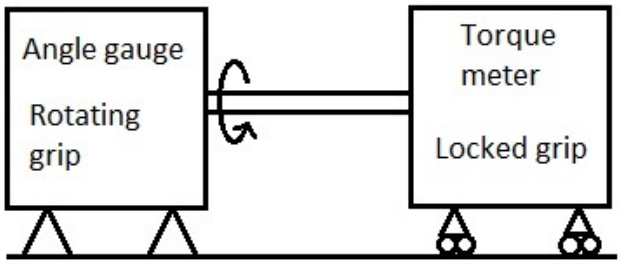

Figure 6.1: A schematic picture of a torsion testing machine.

The hardware used in this experiment was a modification of a machine designed for testing screws and contains all the necessary parts as depicted in figure 6.1. The modification was only the grips, which were originally adapted for screws only. Instead of the grip for the threaded end a plate with a hexagonal hole was screwed to the load cell of the torque meter. The complete set up is shown in figures 6.2-6.3.

The test bars used were designed as a combination of a regular test bar for tensile testing and machined test pieces used for torsion testing of screws. The mechanical design is shown in figure B.1 in appendix B. One bar was taken from crank four of each crankshaft, but as the test failed for crankshaft E two new test bars were manufactured from crank five. Crankshaft E was thus tested at a later time but with identical set-up.

The test bars were attached to the grips and the rotating grip was rotated with the speed of 10°/s until failure. The torque measured in Nm was plotted as function of rotated angle.

6.1.1 Results

The resulting "stress-strain-curves" are presented in figure 6.4. The units on the axes are rotated angle and torque in Nm, but because of the tight tolerances of the test bars the results are believed to be analogous to a plot of calculated shear stress and shear strain. When testing crankshaft A the first test ended at 132Nm because of an incorrectly set overload protection in the load cell. Thus there are two curves for this test bar; the black one for the first test and the blue for the second test. Of course the pre-straining affected the test bar, as can be seen in the increased yield strength, but the original yield strength was captured in the first test. The ultimate shear strength captured in the second test is not believed to have changed by the pre-straining, and the rotation at failure should be the same as in the second test plus the ten to twenty degrees that was rotated plastically in the first test.

All specimens follow the same curve until the onset of plasticity, which means that the shear modulus as expected is the same for all crankshafts. Also the onset of plasticity

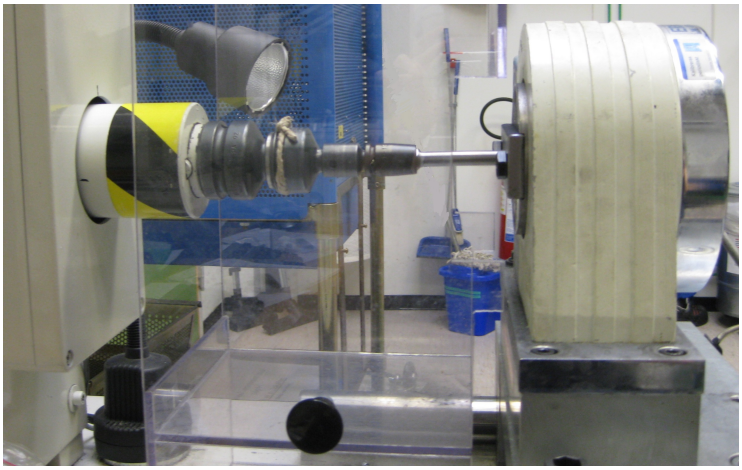

Figure 6.2: Picture of the torsion testing machine used with mounted sample.

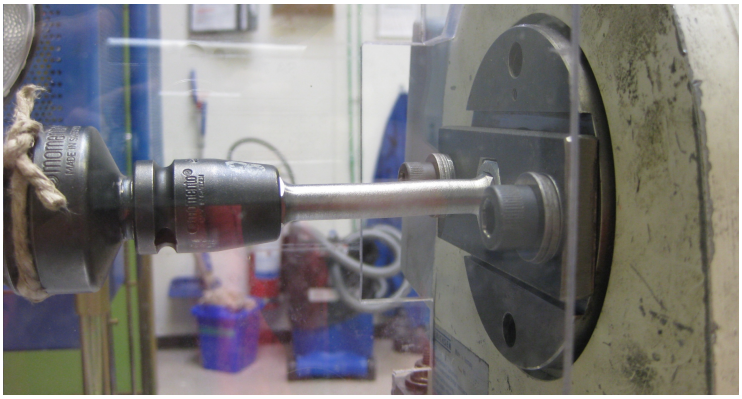

Figure 6.3: Close up of the set up with the adapted grip on the right side during testing. The bar plasticizes after being rotated almost 360°.

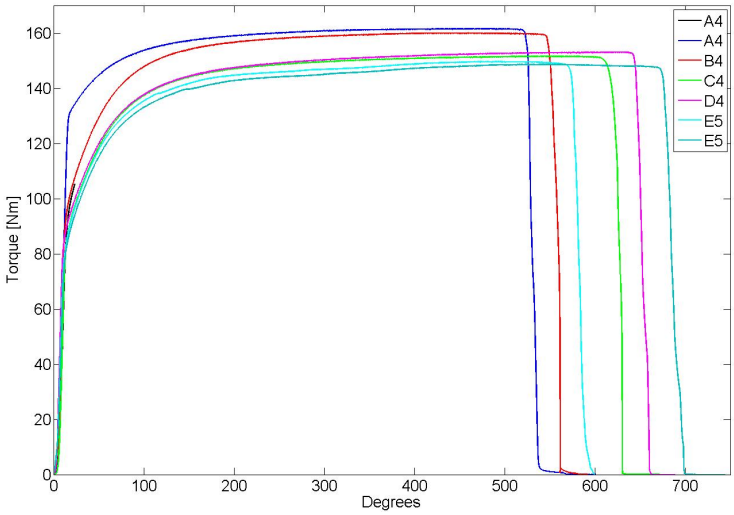

Figure 6.4: Results from the torsion test. All test bars were taken from crank four except on crankshaft E where the bars were taken from crank five.

occurs around 90Nm for all test bars. Beyond the yield point obvious differences are seen. The test bars exhibit two distinct ultimate torque levels of around 160 Nm for crankshafts A and B, and of around 150 Nm for crankshafts C,D and E. This means that the ultimate shear strength levels are higher in the latter case. Large variations are seen in rotation at failure, with A and B rupturing at lower angles than the other samples.

A,B and C are supplied by S1 with A belonging to a separate charge, and the others are supplied by S2. It is thus peculiar that A and B, from different charges, have similar curves while C behaves more like the crankshafts from S2. The lower ultimate shear strength of C could be explained by some local variation or defect that localizes the stress at an earlier stage, but it is counter intuitive that such an defect would allow the increased rotation at failure. One could however dispute the importance of rotation at failure considering the 100°-difference between the first and second specimen from crankshaft E.

The conclusion drawn from the torsion testing is that there seems to be some small difference in shearing properties between the materials from the two suppliers, with S1's crankshafts being more resilient to shear, which could lead to lower shear ductility. However, exceptions or variations do exist, and a greater number of tests would have to be done to draw any certain conclusions.

6.2 Charpy impact testing

The Charpy impact test measures the apparent energy required to break a rectangular specimen. This inmpact energy varies with temperature because the percentage of the fracture that occurs through ductile fracture increases with temperature and ductile fracture is more energy consuming than brittle fracture. By looking at the fracture surface the fraction of ductile versus brittle fracture can be determined. The purpose of this test was that it, together with the results from the torsion test, would give insight into the ductility of the two materials through revealing its tendency to react in a ductile manner.

The Charpy impact test consists of a test piece which is hit by a pendulum. The energy lost in breaking the specimen is calculated as the difference in potential energy of the pendulum before and after the impact. Two pieces measuring 10x10x55 mm were taken from the bulk of crank four of each crankshaft. All tests were performed at room temperature. Also, the specimens were expected to have some fraction of ductile fracture at room temperature which could then be compared. The test was performed by Swerea Kimab according to standard ISO 148 (v-notch specimens).

6.2.1 Results

The impact energies are listed in table 6.1. All fractures were found to be 100% brittle.

Table 6.1: Results from the Charpy impact test

Crankshaft	Piece 1	Piece 2
A	14	10
B	10	11
C	13	10
D	10	9
E	8	9

The results showed that the specimen did not behave as expected, but breaking with 100% brittle fracture. This makes comparison of the ductile tendencies impossible, therefore the choice of room temperature was wrong, i.e. below the DBTT. The impact energy was lower for the crankshafts from S2, but the difference in impact energy was not larger than the differences among different specimens of the same supplier. Thus, the only possible conclusion from this test is that the materials have approximately the same impact energies in the brittle regime.

6.3 Tensile testing of hardened material

A tensile test of the bulk material would not have to be done since the suppliers did that and provided the results in the material certificates, see table 3.2. However, the grinding is not applied to the bulk metal but to the hardened surface. Hence, other results from a tensile test – e.g. ultimate tensile strength, yield strength etc – would of course thus be of interest to measure for the surface material. In particular, the fact that one supplier's crankshafts are more ductile as the bulk material does not necessarily mean that the martensitic surface is more ductile.

Thus, two tensile test bars were manufactured from the bulk material of the sixth crank of each crankshaft according to drawings in standard SS 112113, test bar type 5C50. The bar had a diameter of 5 mm and threaded ends. The test bars were then induction hardened, quenched in 10% polymer solution and tempered at 180° for 1h. This mimics the actual heat treatment of the crankshafts. The average hardening depth of the crankshafts' washers (3 mm) is close to the hardening depth of the test bar (diameter/2=2.5mm), which should result in the test bar having as similar composition to the crankshaft surface material as possible. After the heat treatment they were grinded into the final dimensions to remove any shape errors caused by the heat treatment. The strain rate at the testing was 0.06mm/s.

6.3.1 Results

The results are shown in figure 6.5 and table 6.2. One of the measurements on crankshaft A is missing as the test bar broke while it was being manufactured. It is unknown what happened, but the fracture surface is all brittle. This might be interesting considering that the other bar (seen from the blue line in figure 6.5) also broke in a relatively brittle manner, although some cup and cone behavior was visible, indicating some plasticity. One of the bars from crankshaft C broke in the threading, possibly because it was not perfectly aligned.

The other curves are fairly similar until close to their ultimate tensile strengths level. The maximum difference in UTS is about 100 MPa (between B and D), and all have area reductions of around 45% except crankshaft E. No differences can be seen between the two suppliers whatsoever, but it is suspicious that the ductility should increase for all crankshafts compared to the as delivered state (see table **??**) but E when the material is hardened. The hardening should make the test bars really brittle despite the tempering, more similar to B or maybe even A. Thus there was probably something wrong with the test bars, something that might be worth examining in the future.

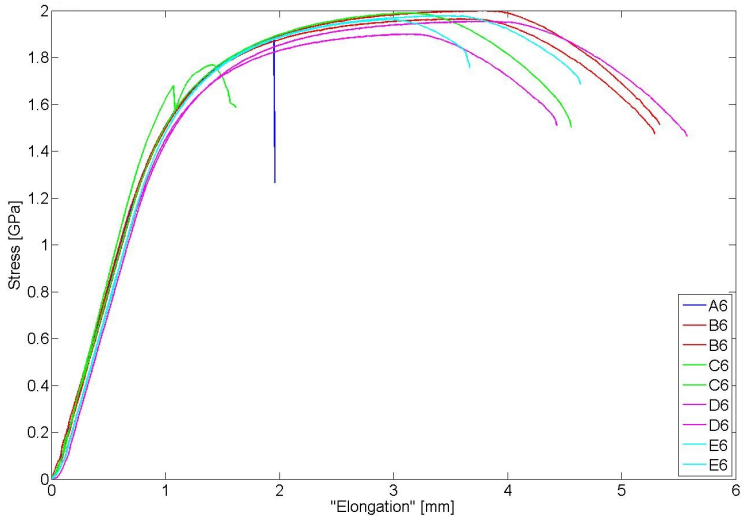

Figure 6.5: Results from the tensile test of hardened material. All test bars were taken from crank six. The "elongation" is really the movement of the test machine grips because most bars failed where the strain meter was attached to the bar, thus resulting in erroneous strain measurements. Thus it contains the elongation of the entire bar and not just the waist.

Table 6.2: Material data from the tensile test of hardened materials.

Crankshaft	UTS [GPa]	Area reduction [%]
A	1.88	0
B	1.96	48
B	2.00	46
C	1.99	45
D	1.90	43
D	1.95	48
E	1.98	33
E	1.96	22

6.4 Summary of experiments part 3

Not many conclusions can be drawn from part 3, with the Charpy impact test failing for choice of temperature and the tensile test leaving only suspicions of bad test bars. The torsion test yielded two distinct groups of crankshafts, with crankshaft E again being the wild card, maybe because a different crank was used. All in all the theory of a higher ductility in crankshafts D and E has not been as well supported as was hoped, but it has certainly not been gainsaid either.

7 Concluding remarks and future work

The purpose of this thesis has been to shed light on why the Barkhausen response is different for two of Scania's present suppliers of crankshaft. The work has led to two primary conclusions. Firstly that the only major difference found between the two materials is the bulk ductility. This may have major consequences for the grinding performance of the materials, leading to greater heat generation and increasing the risk for grinding burns in the crankshafts from S2. But more research still have to be done to establish what causes this ductility difference. If the ductility difference is caused by e.g differences in the distribution of precipitates too small to see with optical microscopy then this effects the BNA in itself (see subsection 2.3.3). Indeed the small difference in formation of bainite during cooling might imply some underlying difference in the homogeneity of alloying elements that then of course would be detected by the Barkhausen Noise technique. Also it will have to be established that the bulk ductility difference in fact does transfer to the hardened surface layer. Furthermore the mechanism in which the ductile material affects the grinding wheel, the chips clogging the pores, has to be confirmed.

Secondly another conclusion is that the material parameter that seem to have the greatest influence on the Barkhausen response on crankshafts is the residual stresses. Although other parameters, e.g. hardness, also influence the signal the residual stresses seem to be the major factor in this application where microstructural factors seem relatively constant. One reason for is the shallow measurement depth of the Barkhausen technique. The measurements of other material parameters are usually conducted at greater depths and thus do not correlate as well with the surface BNA. Apart from the residual stress test, the only other test performed within this thesis project that truly measures within the Barkhausen measurement depth is the optical microstructure examination.

Suggestions for future work is:

- Examine the mechanical properties of the hardened layer, especially the ductility. Establish the cause for the ductility difference and check that this is not enough to explain the difference in BNA.
  There were difficulties with the tensile testing performed within this thesis because of the test bars used. The test method for this have to be improved concerning the hardening of the test bars, making sure that the bars are actually representative for the hardened layer of the crankshafts.

- Investigate in detail how the material interacts with the grinding wheel.
  Affirm or disaffirm the current hypothesis of chips clogging the pores because of the higher ductility of one of the suppliers' crankshafts.

- Assuming that the crankshafts do differ in ductility, do grinding tests changing the grinding parameters as one would for a more ductile material. Could results from previous grinding tests be explained by a difference in ductility?

A Barkhausen Noise results

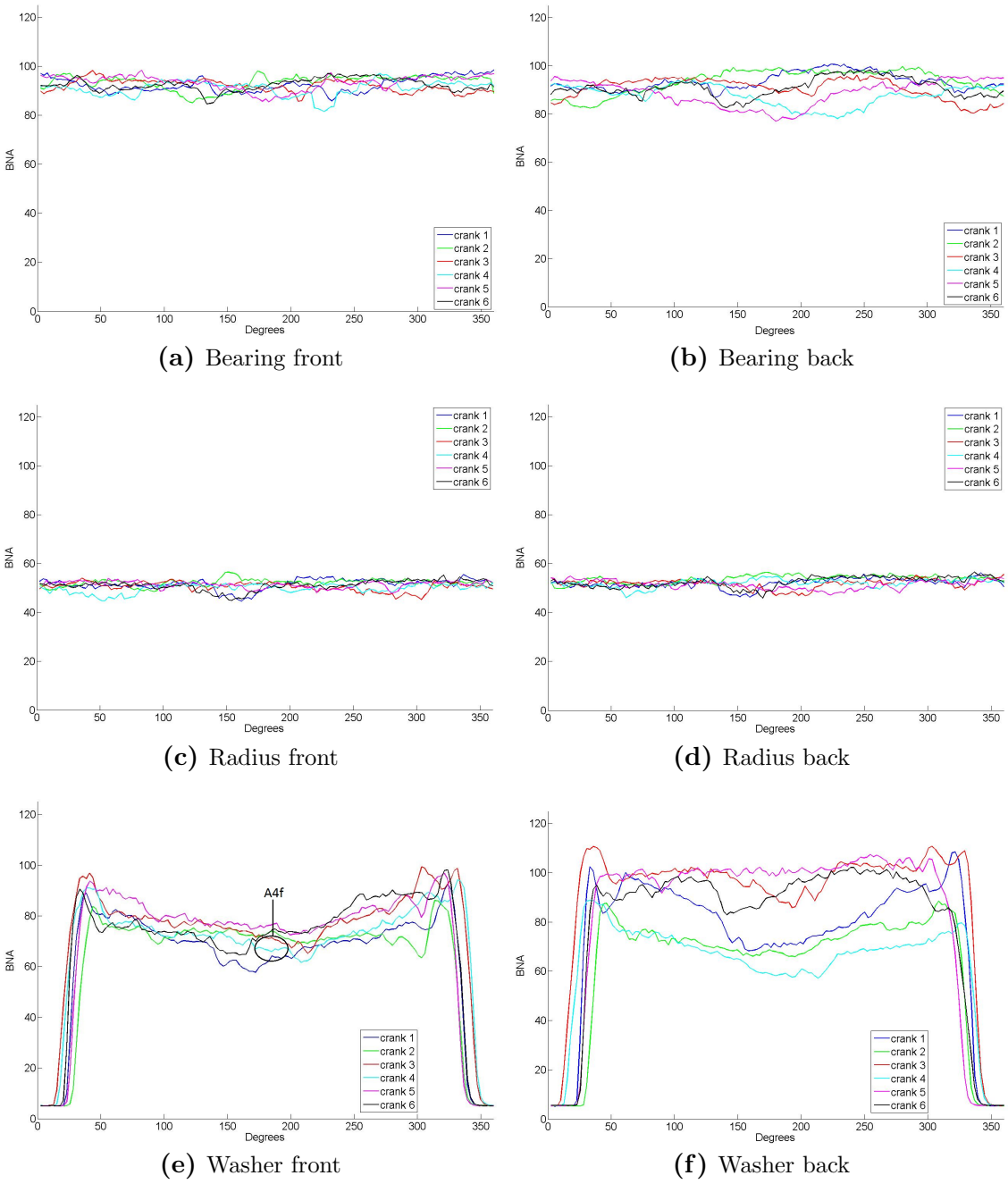

(a) Bearing front

(b) Bearing back

(c) Radius front

(d) Radius back

(e) Washer front

(f) Washer back

Figure A.1: Barkhausen noise curves obtained from crankshaft A.

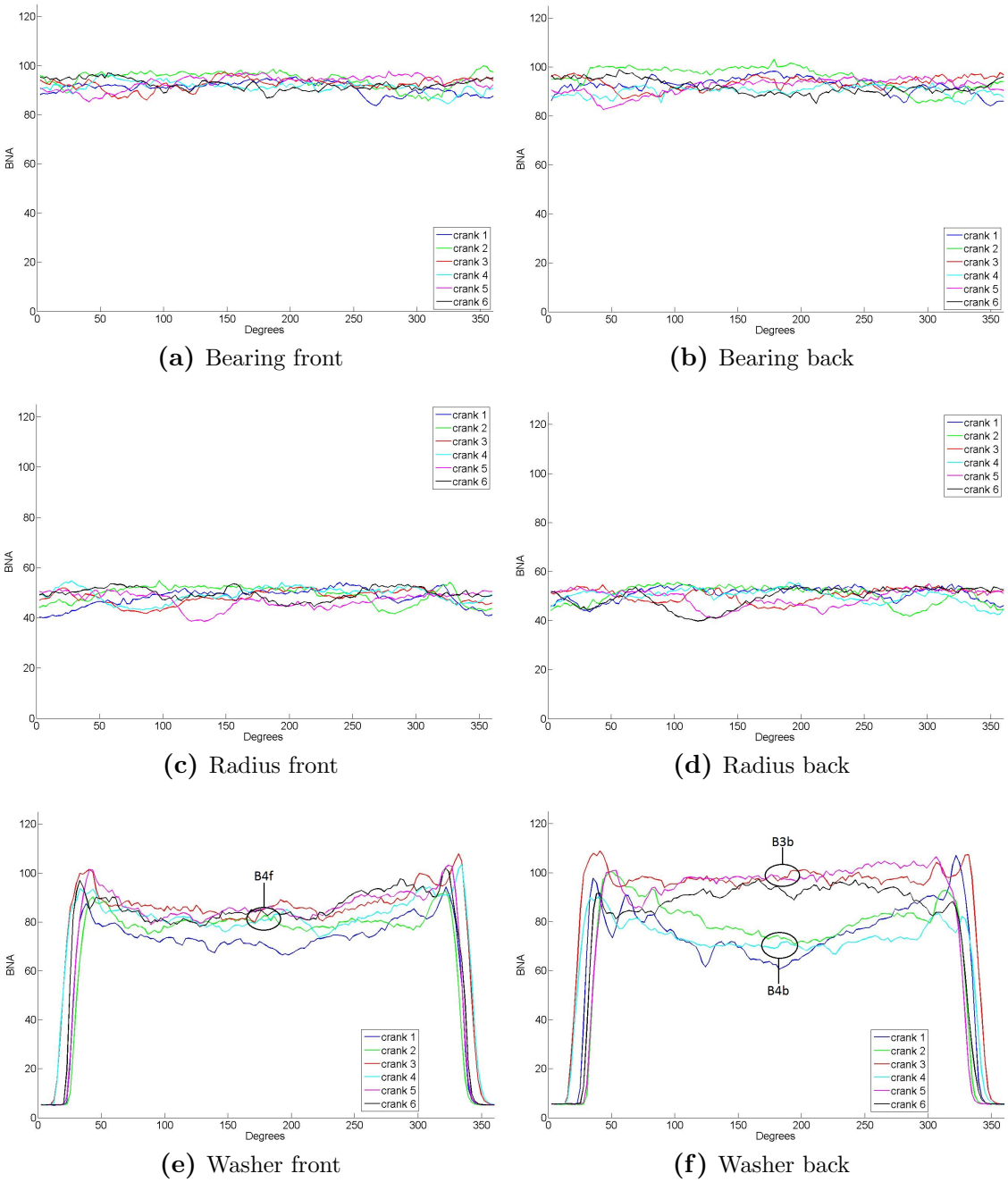

(a) Bearing front

(b) Bearing back

(c) Radius front

(d) Radius back

(e) Washer front

(f) Washer back

Figure A.2: Barkhausen noise curves obtained from crankshaft B.

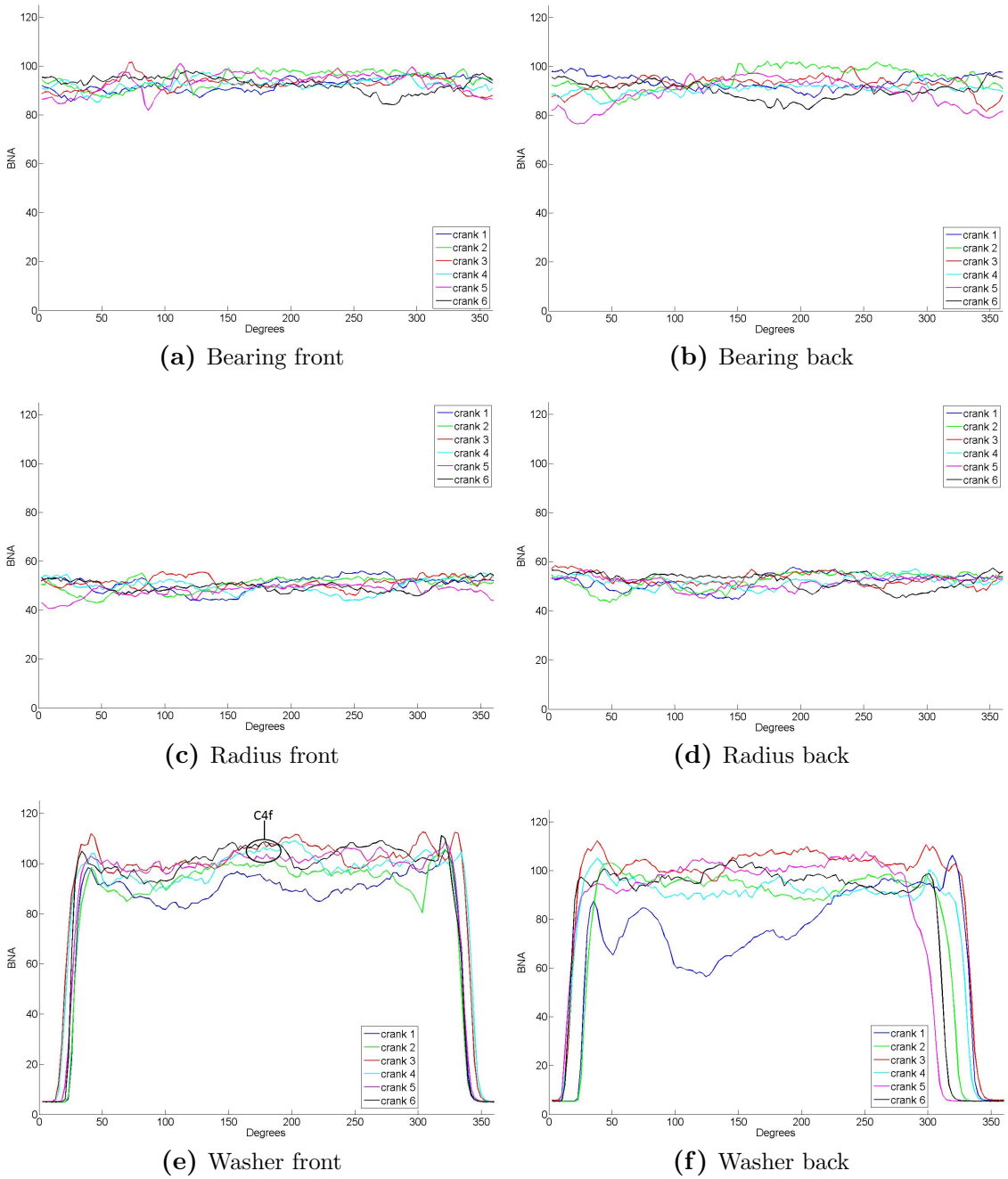

(a) Bearing front

(b) Bearing back

(c) Radius front

(d) Radius back

(e) Washer front

(f) Washer back

Figure A.3: Barkhausen noise curves obtained from crankshaft C.

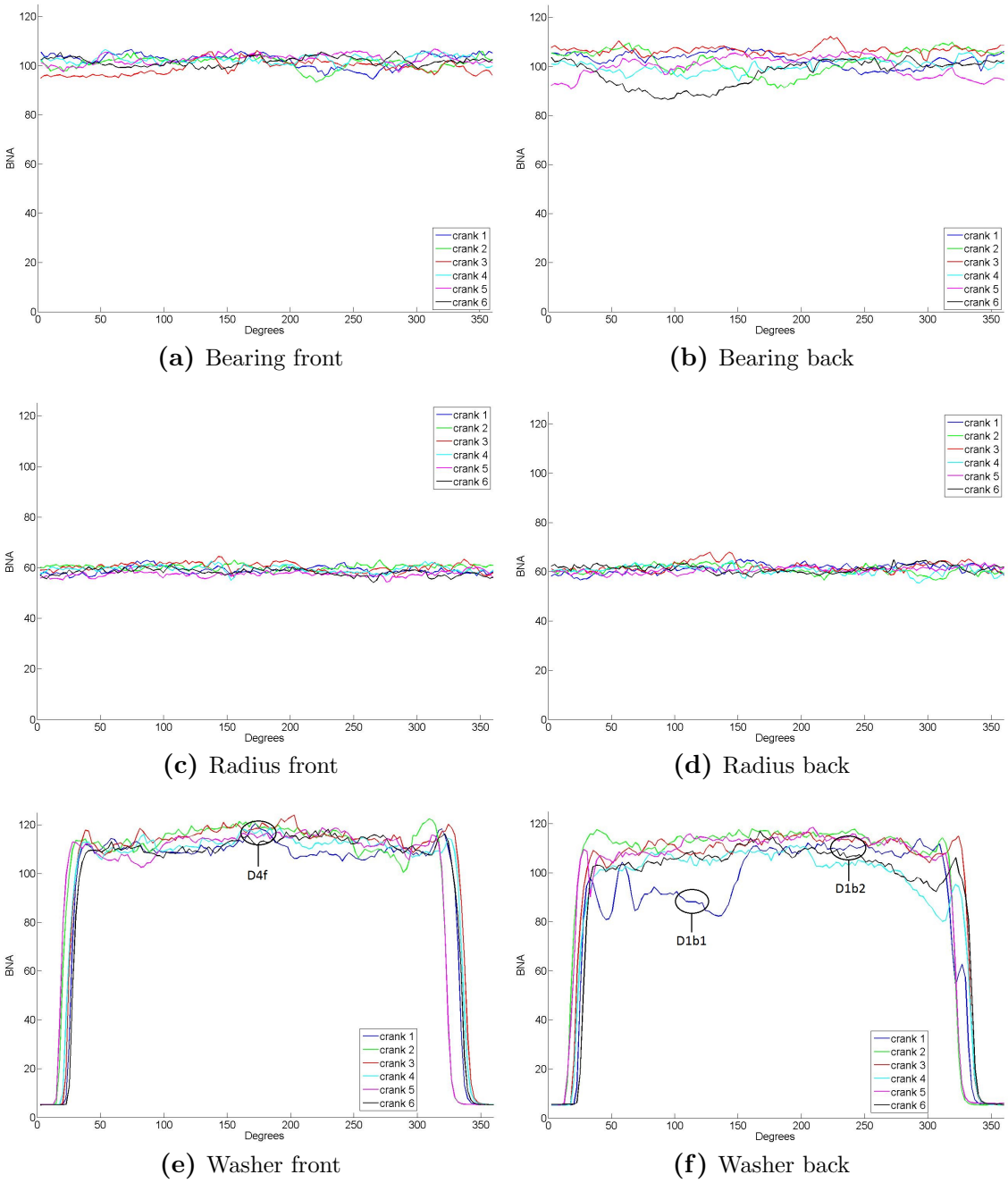

(a) Bearing front

(b) Bearing back

(c) Radius front

(d) Radius back

(e) Washer front

(f) Washer back

Figure A.4: Barkhausen noise curves obtained from crankshaft D.

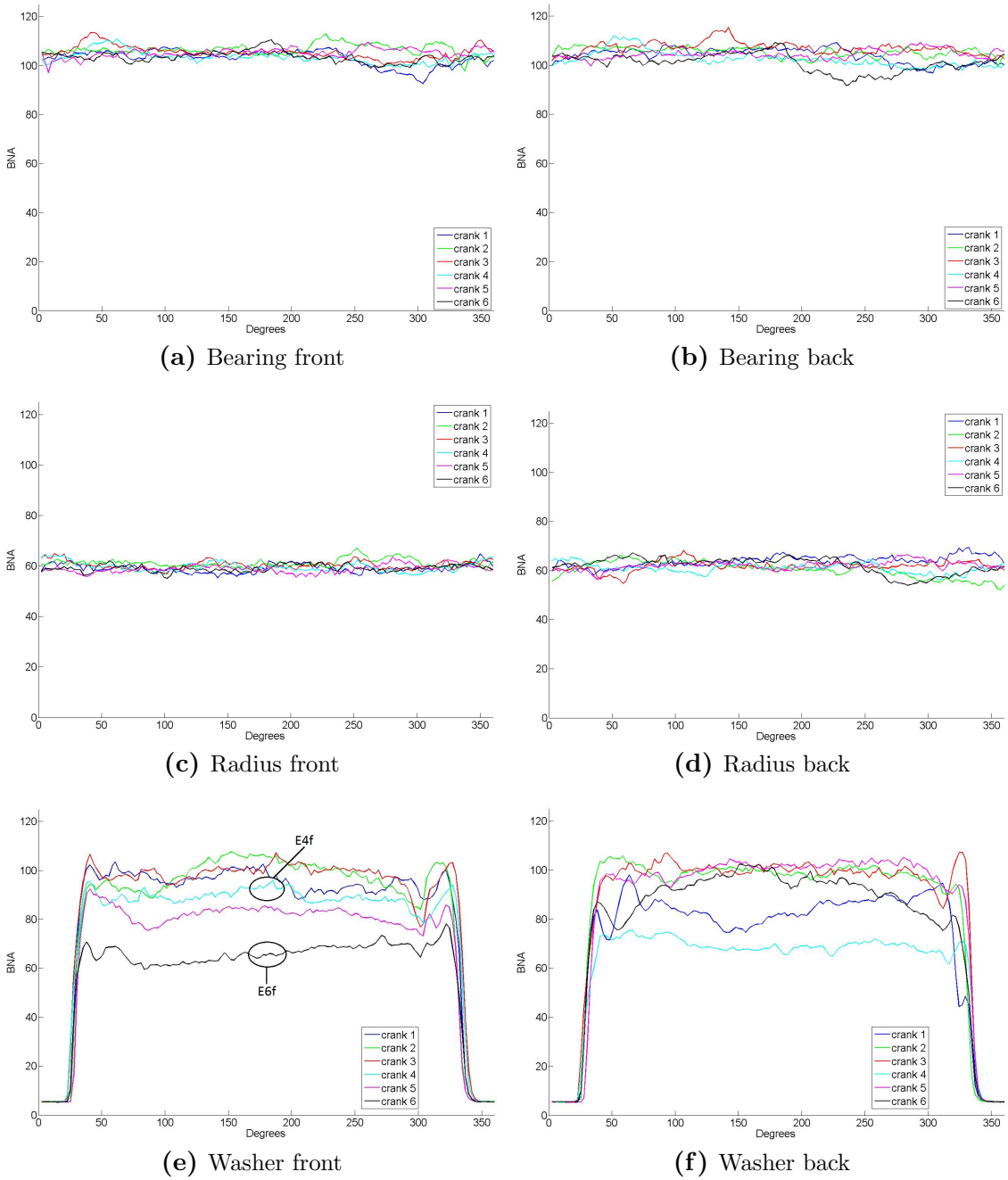

(a) Bearing front

(b) Bearing back

(c) Radius front

(d) Radius back

(e) Washer front

(f) Washer back

Figure A.5: Barkhausen noise curves obtained from crankshaft E.

B Torsion test bar

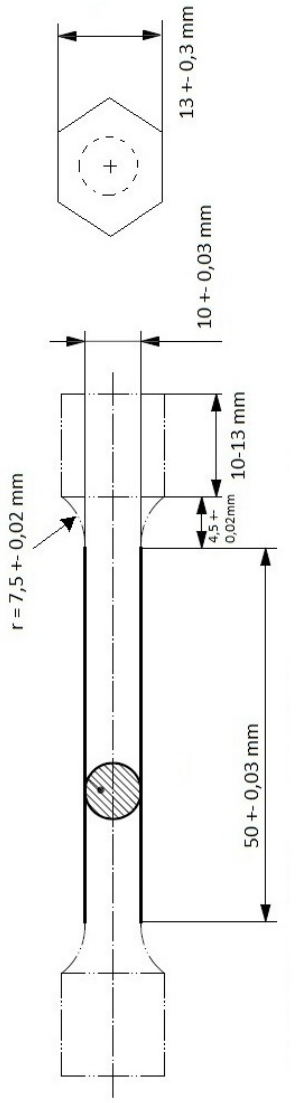

Figure B.1: Torsion test bar used in the torsion tests in section 6.1.

References

[1] Key figures scania (2010). `http://www.scania.com/scania-group/scania-in-brief/key-figures/`, 2012-02-10.

[2] A.P. Parakka, D.C. Jiles, H. Gupta, and S. Jalics. Effects of surface condition on Barkhausen emissions from steel. *Journal of Applied Physics*, 79:6045–6046, 1996.

[3] H. Gupta, M. Zhang, and A.P. Parakka. Barkhausen effect in ground steels. *Acta Materialia*, 5:1917–1921, 1997.

[4] M. Meyers and K. Chawla. *Mechanical Behaviour of Materials 2nd edition*. Cambridge University Press, Cambridge, UK, 2009.

[5] R.E. Hummel. *Electronic Properties of Materials 3rd edition*. Springer Science+Business Media Inc., New York, USA, 2005.

[6] J. Kameda and R. Ranjan. Nondestructive evaluation of steels using acoustic and magnetic Barkhausen signals – I. Effect of carbide precipitation and hardness. *Acta Metallurgica*, 35:1515–1526, 1987.

[7] J. Kameda and R. Ranjan. Nondestructive evaluation of steels using acoustic and magnetic Barkhausen signals – II. Effect of intergranular impurity segregations. *Acta Metallurgica*, 35:1527–1531, 1987.

[8] P. Cizeau, S. Zapperi, G. Durin, and H. Eugene Stanley. Dynamics of a ferromagnetic domain wall and the Barkhausen effect. *Physical Review Letters*, 23:4669–4672, 1997.

[9] S. Zapperi and P. Cizeau. Dynamics of a ferromagnetic domain wall: Avalanches, depinning transition, and the Barkhausen effect. *Physical Review B*, 58:6353–6366, 1998.

[10] J.A. Pérez-Benitez, J. Capó-Sánchez, and L. R. Padovese. Modelling of the Barkhausen jump in low carbon steel. *Journal of Applied Physics*, 103:043910–1–043910–6, 2008.

[11] Z. D. Wang, Y. Gu, and Y. S. Wang. A review of three magnetic NDT techniques. *Journal of Magnetism and Magnetic Materials*, 324:382–388, 2011.

[12] S. Tiitto, M. Otala, and S. Säynäjäkangas. Non-destructive measurement of steel grain size. *Non Destructive Testing*, 9:117–120, 1976.

[13] S. Tiitto. Influence of elastic and plastic strain on the magnetization process in Fe-3.5%Si. *IEEE Transactions on Magnetics*, MAG-12:855–857, 1976.

[14] S. Tiitto. On the mechanism of magnetization transitions in steel. *IEEE Transactions on Magnetics*, MAG-14:527–529, 1978.

[15] B. Alessandro, C. Beatrice, G. Bertotti, and A. Montorsi. Domain wall dynamics and Barkhausen effect in metallic ferromagnetic materials I. Theory. *Journal of Applied Physics*, 68:2901–2907, 1990.

[16] J.A. Pérez-Benitez, J. Capó-Sánchez, J. Anglada-Riviera, and L. R. Padovese. A model for the influence of microstructural defects on magnetic Barkhausen noise in plain steels. *Journal of Magnetism and Magnetic Materials*, 288:433–442, 2005.

[17] J.A. Pérez-Benitez and L. R. Padovese. Study of the influence of simultaneous variation of magnetic material microstructural features on domain wall dynamics. *Journal of Magnetism and Magnetic Materials*, 322:3101–3105, 2010.

[18] Relationship of Barkhausen and residual stresses, hardness and etching at crankshaft washers. Scania Technical Report 7006988, 2008.

[19] Technical relationships with Barkhausen noise for camshafts, part no.1. Scania, TZMM 99/171, 1999.